BASIC RESEARCH

WILEY

Modeling essential hypertension with a closed-loop mathematical model for the entire human circulation

Morena Celant[1] | **Eleuterio F. Toro[2]** | **Giulia Bertaglia[3]** | **Susanna Cozzio[4]** | **Valerio Caleffi[5]** | **Alessandro Valiani[5]** | **Pablo J. Blanco[6]** | **Lucas O. Müller[1]**

[1]Department of Mathematics, University of Trento, Trento, Italy

[2]Laboratory of Applied Mathematics, DICAM, University of Trento, Trento, Italy

[3]Department of Environmental and Prevention Sciences, University of Ferrara, Ferrara, Italy

[4]U.O. di Medicina Interna, Ospedale di Rovereto, Azienda Sanitaria per i Servizi Provinciali di Trento, Trento, Italy

[5]Department of Engineering, University of Ferrara, Ferrara, Italy

[6]National Laboratory for Scientific Computing, Petròpolis, Brazil

Correspondence

Lucas O. Müller, Department of Mathematics, University of Trento, Trento, Italy.
Email: lucas.muller@unitn.it

Abstract

Arterial hypertension, defined as an increase in systemic arterial pressure, is a major risk factor for the development of diseases affecting the cardiovascular system. Every year, 9.4 million deaths worldwide are caused by complications arising from hypertension. Despite well-established approaches to diagnosis and treatment, fewer than half of all hypertensive patients have adequately controlled blood pressure. In this scenario, computational models of hypertension can be a practical approach for better quantifying the role played by different components of the cardiovascular system in the determination of this condition. In the present work we adopt a global closed-loop multi-scale mathematical model for the entire human circulation to reproduce a hypertensive scenario. In particular, we modify the model to reproduce alterations in the cardiovascular system that are cause and/or consequence of the hypertensive state. The adaptation does not only affect large systemic arteries and the heart but also the microcirculation, the pulmonary circulation and the venous system. Model outputs for the hypertensive scenario are validated through assessment of computational results against current knowledge on the impact of hypertension on the cardiovascular system.

KEYWORDS

arterial hypertension, arterial pressure regulation, global closed-loop model

1 | INTRODUCTION

Essential, or primary, or idiopathic arterial hypertension is historically defined as a chronic, usually progressive, raised arterial blood pressure.[1] According to the guidelines of the European Society of Hypertension,[2] hypertension is defined as an office systolic blood pressure >140 and/or diastolic blood pressure >90 mm Hg. Arterial hypertension is by far one of the most important sources of morbidity and mortality in the world.[3] It affects approximately 40%–45% of the world population aged >25 years (1.13 billion in 2015[2]) with a global age-standardized prevalence of 24% and 20% in men and women, respectively.[2] Moreover, hypertension becomes progressively more common with advancing age, with a prevalence >60% in people aged >60 years. As populations age and adopt more sedentary lifestyles, prevalence of hypertension continues to rise and is expected to affect more than 1.5 billion people by 2025.[2] It has been estimated that

complications arising from hypertension account for 9.4 million deaths worldwide every year[3]; examples of hypertension-related diseases are ischaemic heart disease, heart failure, atrial fibrillation, chronic kidney disease, peripheral artery disease, stroke and cognitive decline, to name but a few.

The body is endowed with many interrelated arterial pressure regulating mechanisms. Each one of them performs a specific function to provide both short-term and long-term arterial pressure regulation.[4,5] The first line of reaction against acute changes in arterial pressure is the nervous control system; this class of regulatory mechanisms responds in seconds to pressure changes and includes the baroreceptor feedback mechanism, the central nervous system ischaemic mechanism and the chemoreceptor mechanism. The nervous mechanisms act on constriction/dilation of most peripheral arterioles, on contractility of the heart and on vein reservoir properties to almost instantly reset arterial pressure to a physiologically adequate value. After a few minutes following acute arterial pressure changes, other mechanisms are activated: the renin-angiotensin vasoconstrictor mechanism, stress-relaxation of the vasculature, and shift of fluid through the tissue capillary walls in and out of the circulation to readjust the blood volume as needed. The long-term (over days, months, and years) pressure regulation is achieved mainly by kidney mechanisms through renal-body fluids pressure-volume control and its interaction with other factors, such as the renin-angiotensin system with the aldosterone mechanism. How these regulatory mechanisms contribute in the development and progression of the hypertensive disease remains the subject of debate.[4,6–8]

In this unclear and broad scenario, computational models can be a practical approach for better quantifying the haemodynamic effects of cardiovascular properties in this medical condition. An early, seminal contribution in this field is due to Guyton in the early 70s,[4] which was concerned with the system analysis of arterial pressure regulation and hypertension. The model presented in Reference 4 consists of several hundred algebraic and ordinary differential equations that incorporate the main components of the vascular system, their interaction with extracellular fluid volume and detailed regulatory mechanisms. Departing from the pioneering Guyton's contributions, other mathematical models have been developed to provide a more comprehensive representation of the entire circulation and its control by other influences, including the central nervous system.[6,9–11] These mathematical models describe the effects of regulatory systems on the circulation, the heart, and the kidney by means of systems of ordinary differential and algebraic equations, aiming at increasing our understanding of long-term control of arterial pressure.

Other approaches in mathematical modeling of arterial hypertension have focused on particular districts of the cardiovascular system. For example, Segers et al.[12] studied the heart-arterial interaction in hypertension-induced left ventricular hypertrophy using a left ventricle time-varying elastance model coupled to a 4-element lumped parameter model of the systemic arterial system. One-dimensional models of the arterial system have been widely employed to study arterial haemodynamics under various pathophysiological conditions; this kind of models are suitable for studying wave propagation phenomena under aging and hypertensive conditions. Two exemplary papers along these lines are.[13,14] In the first one, the hypothesis that increased pulse wave reflection and altered backward waveform morphology contribute to increased pulse pressure in subjects with higher pulse pressure was tested with the help of numerical modeling (55-segment 1D arterial network model) to confirm the interpretation of the experimental results. In the second paper, one-dimensional computational modeling was used to provide a database of arterial pulse waves to span a range of cardiovascular conditions, representative of a population of healthy adults. Another relevant contribution is due to Blanco et al.,[15] in which an Anatomically Detailed Arterial Network (ADAN) model was used to study the role of hypertension in cerebral small vessel disease. Model parameters were modified to consider structural changes in arterial vessels in the hypertensive scenario. All of these 1D models are open-loop models. The first works that incorporated a closed-loop network, and thus a description of the venous district, were put forward by Liang et al.[16] and by Canuto et al.[17] As pointed out in Reference 16, mechanical, structural and functional changes may occur in the entire cardiovascular system as a cause or consequence of hypertension. Hence traditional 1D models are not sufficient to satisfactorily describe the remodeling due to hypertension. In this framework, Liang et al.[16] proposed a multi-scale model which integrates the main cardiovascular components prone to alterations in hypertension (such as the heart, large arteries, distal arteries and arterioles) into a unique computational framework that enabled them to explore the determinant cardiovascular factors for haemodynamic variables of concern in the treatment of hypertension. The model of Liang et al. includes a one-dimensional network for major arteries and structured-tree models for small arteries and arterioles; other cardiovascular components are described by zero-dimensional models, included the venous circulation, which is represented by two compartments, one for the upper-body and one for the lower-body. The role played by venous system changes was not explored.

Notably, there is ample clinical evidence showing that the hypertensive setting affects not only large arteries, but also the microcirculation, the heart, the pulmonary circulation and the "low-pressure" system, that is the venous

circulation. In the present work, in order to characterize all main role players of the cardiovascular system in hypertension, we use a global closed-loop mathematical model for the entire human circulation to investigate the hypertensive condition. Such a model departs from the original Müller-Toro model, first proposed in 2014[18,19] and then improved in 2021.[20] It is a geometric multi-scale type model which includes one-dimensional models for blood flow in all major vessels and zero-dimensional lumped-parameters models describing blood flow in the remaining compartments. It includes 323 vessels, comprising arteries and veins; four heart chambers and cardiac valves; 3 compartments for the pulmonary circulation; 31 compartmental models describing the connections between terminal arteries and veins through the microcirculation; 17 venous valves; 21 Starling resistors. Moreover, it is coupled to a simple model based on Reference 21, which describes the intracranial pressure as function of the cerebral blood volume; this intracranial pressure serves as the external pressure of all the intracranial districts. Concerning physiological control systems, this global mathematical model incorporates a cerebral autoregulation model, which aims at maintaining adequate and stable cerebral blood flow during changes in blood pressure acting on dilatation or contraction of arterioles and capillaries,[22,23] and a model for short-term regulation of pressure, which considers the activity of high- and low-pressure baroreceptors.[24,25] Based on available physiological knowledge on the hypertensive state, we modify our model to incorporate structural and functional differences affecting the cardiovascular system in this pathological condition, aiming at computationally reproducing a functioning hypertensive cardiovascular system. The resulting modeling framework is validated via the comparison of model outputs against experimental evidence on the functioning of the hypertensive cardiovascular system. Figure 1 summarizes schematically the structure of the present work.

The rest of the paper is structured as follows. Section 2 summarizes the main features of the cardiovascular model on which this work is based and then it describes the modifications on the model parameters to simulate the hypertensive condition. Section 3 presents main computational results on normotensive and hypertensive conditions. Computed data are validated and discussed with respect to clinical measurements reported in the literature in Section 4. Finally, Section 5 includes concluding remarks, comments on limitations of the present model and possible future developments.

2 | METHODS

In this section, we present the global closed-loop mathematical model of the entire human circulation and its adaptation to arterial hypertension remodeling. All the main ingredients of the global model were described in detail in previous works and are here briefly summarized. Appendix A includes Table A1, which features a summary of all the main equations of our model and Table A2, which reports all parameter values, including references from previous works where parameters were originally proposed. The only missing parameters regard vessel lengths, diameters and connectivity, which can be found in Reference 20. We refer the reader to References 18–20,25 for further details. Concerning the remodeling due to hypertension, we describe how the model parameters are changed based on clinical measurements reported in the literature.

2.1 | Mathematical model of the cardiovascular system

We model blood flow in the entire human circulation by means of a geometric multi-scale type model which includes one-dimensional models for major vessels and compartmental models for the remaining components.

2.1.1 | Arteries and veins

Blood flow in major vessels, arteries and veins, is modeled using a 1D system of partial differential equations based on averaging the incompressible Navier–Stokes equations over the vessel's cross-sectional area, while neglecting body forces such as gravity. The resulting system expressing conservation of mass and balance of momentum is given by

$$\begin{cases} \partial_t A + \partial_x q = 0, \\ \partial_t q + \partial_x \left(\dfrac{q^2}{A} \right) + \dfrac{A}{\rho} \partial_x p = -f. \end{cases} \tag{1}$$
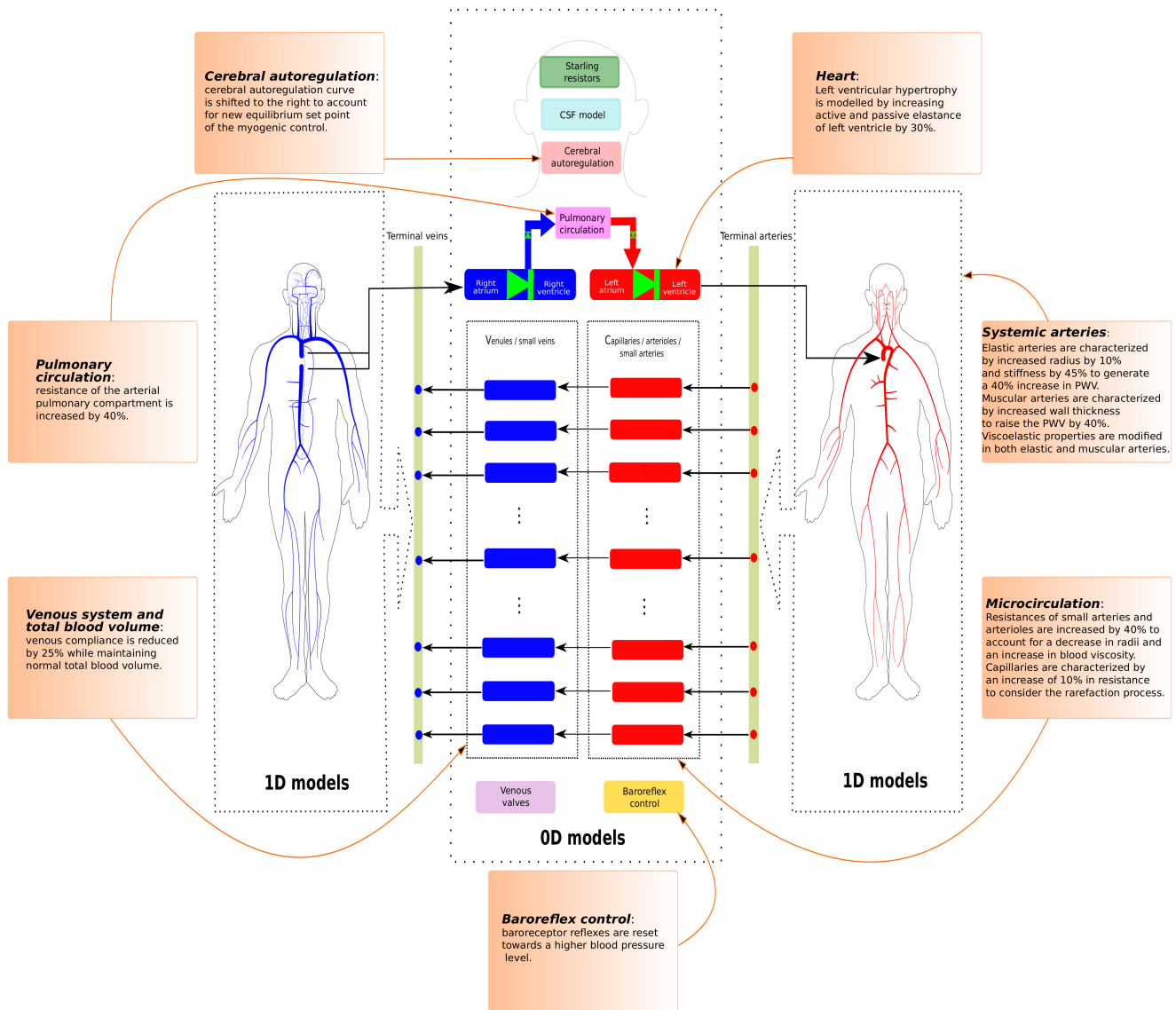
FIGURE 1   Schematic representation of the global mathematical model of the circulation and its adaptation in hypertensive condition. 1D model refers to networks of major arteries and veins, which are modeled using evolutionary partial differential equations, providing space- and time-resolved blood pressure and flow. Rectangles represent lumped-parameter models, which are used to describe the heart chambers, the pulmonary circulation, the microcirculation, as well as valves, Starling resistors and intracranial pressure dynamics. Two regulatory systems are also incorporated: cerebral autoregulation and baroreflex control. Such compartments and regulatory processes are modeled using ordinary differential equations (0D model), which provide time-resolved haemodynamic variables.

The three unknowns are $A(x,t)$, the cross-section's area of the vessel's lumen, $q(x,t)$, the blood flow rate, and $p(x,t)$, the cross-sectionally averaged internal pressure. ρ is the blood density and f is the friction force per unit length of the tube (see Equation A5 in Table A1). To close the system, we adopt a pressure-area relation based on the Kelvin-Voigt model, which describes the viscoelastic nature of vessel walls

$$p(x,t) = p_{ext}(x,t) + \underbrace{K(x)\left(\left(\frac{A(x,t)}{A_0(x)}\right)^m - \left(\frac{A(x,t)}{A_0(x)}\right)^n\right) + P_0}_{\text{Elastic term}} + \underbrace{\frac{\Gamma(x)}{A_0\sqrt{A}}\partial_t A}_{\text{Viscoelastic term}} , \tag{2}$$

where, $A_0(x)$ is the vessel cross-sectional area at equilibrium, P_0 the reference pressure, $p_{ext}(x)$ the external pressure. The parameters m and n are two real numbers that can be derived from experimental measurements; throughout this

work, we assume $m = 10$ and $n = -1.5$ for both arteries and veins. In previous versions of this mathematical work,[19,20,25] we usually assumed $m = 0.5$ and $n = 0$ for arteries; generally one needs to choose $m > 0$ and n in $[-2, 0]$ in order to preserve desirable mathematical properties of the PDE system.[33] However, in Reference 34, direct estimation of m and n in ovine and human arteries revealed that values of m greater than 4 and values of n smaller than -0.4 are more appropriate for the representation of the hyperelastic nature of the vessels wall and their collapsing behavior; real vessels tend to become stiffer as deformations grow, which is not satisfied if the value $m = 0.5$ is adopted. Since we are interested in hypertension remodeling and hence vessels' deformations over a wide blood pressure range, we believe that more realistic values of these constants need to be used. $K(x)$ is the vessel stiffness; it accounts for mechanical and geometrical properties of the vessel. In this work its value is linked to the observed relation between the speed of propagation of small perturbations and vessel diameters. Such relation was observed in arteries[35] and veins,[36] and was previously used to characterize the mechanical properties in one-dimensional models, see for example References 37,38. The precise definition of c_0 and its dependence on vessel diameter is provided in full detail in Reference 20. $\Gamma(x)$ is a constant related to the viscoelastic properties of the vessel wall and it is chosen following,[39] as

$$\Gamma(x) = \frac{2}{3}\sqrt{\pi}\gamma h_0(x), \tag{3}$$

where, γ is the wall viscosity and $h_0(x)$ is the wall thickness. The value of these parameters are chosen such that the hysteresis of pressure-area plots in peripheral arteries and veins reproduces physiological observations. We refer the reader to Reference 20 for more details about the chosen parameters of the viscoelastic term in the tube law.

When the vessel wall viscoelasticity is incorporated in the model, a second-order spatial derivative of the flow variable in the momentum balance equation arises, turning the problem into an advection–diffusion–reaction problem. Using a relaxation technique, firstly proposed by Cattaneo,[40] we obtain a non-linear hyperbolic PDE system that is solved using a high-order well-balanced non-linear numerical scheme in space and time based on the ADER (Arbitrary high-order DERivatives)[41] finite volume scheme[42–46] and a local time stepping (LTS) approach,[47,48] which is implemented so that the local time step is defined at the level of the vessels. We refer the reader to the works in References 32,41 for an up-to-date review on ADER schemes, to the works in References 44,45 for full details about the high-order well-balanced scheme in the framework of path-conservative schemes, to the works in References 42,43,46 for clarification about the hyperbolic reformulation of the parabolic system incorporating the viscoelastic nature of the vessel wall mechanics, and finally to the works in References 47,48 for the local time-stepping procedure. Considering the coupling of several 1D vessels, we refer the reader to References 19,48–50; the adopted coupling strategy enforces mass conservation and total pressure continuity among vessels sharing a node, while generalized Riemann invariants are used to ensure that coupling conditions and states within one-dimensional domains belong to a smooth solution of the original PDE system.

2.1.2 | Microcirculation

Lumped-parameter models for the microcirculation describe the connection between arteries and veins through arterioles, capillaries and venules; the generic vascular bed model used for all microvasculature beds is based on the three-element Windkessel model. This model is characterized by

- characteristic impedances that couple any number of connecting 1D arteries/veins to lumped-parameter models for the microvasculature (R_{da} or R_{vn}) and regulate the pressure drop between 1D domains and vascular beds;
- peripheral resistance and compliance divided between arterioles (R_{al}, C_{al}) and capillaries (R_{cp}, C_{cp});
- venous compartment characterized by a nonlinear pressure-volume relation with related compliance (C_{vn}) at its basal point.[25]

Moreover, the resistances that are located between capillaries and venules' compartments and the characteristic impedances that couple 1D veins to venules' compartment (R_{cp} and R_{vn}) are nonlinearly related to blood volume variation as described in Reference 25.

2.1.3 | Heart and pulmonary circulation

The heart model uses the "time-varying elastance" model[26,37] to describe the dynamics of relaxation/contraction of the four cardiac chambers, while cardiac valves are modeled as in Reference 27. For each heart chamber, the time-varying elastance $E(t)$ is defined by

$$E(t) = E_A e(t) + E_B, \tag{4}$$

where, E_A and E_B are respectively the maximal contractility at systole and the baseline elastance, while $e(t)$ is the normalized time-varying elastance taken as in Reference 26.

The pulmonary circulation is divided into arteries, capillaries and veins; each compartment is characterized by a pulmonary resistance and a pulmonary inertance that are used for the evolution of the fluid exchange between compartments.

2.1.4 | Venous valves and Starling resistors

Venous circulation is equipped with venous valves, while Starling resistor models are placed at the confluence of cortical veins in the dural sinuses and they prevent the vein collapse maintaining the blood pressure upstream the collapsed segment higher than the intracranial pressure. Both venous valves and Starling resistors are represented by simple ordinary differential equation models that predict their functioning on the basis of the difference between upstream and downstream pressures using the model presented in Reference 27. Concerning Starling resistors, they are placed between cortical veins and corresponding venous sinuses; the pressure difference which regulates the flow across the Starling resistor is evaluated considering the pressure of the cerebral vein (upstream pressure). Equations used to describe valves and Starling resistors are provided in Table A1. For further details on their location and functioning we refer readers to Reference 20.

2.1.5 | Total blood volume

Since total blood volume is of primary importance in the determination of arterial pressure, it is crucial to include a total blood volume control in the global model. To this end, we consider both the stressed and unstressed component of blood volume in both 1D vascular networks and lumped-parameters models for the microcirculation, heart and pulmonary circulation. The unstressed volume is the volume in a compartment when the transmural pressure is equal to zero, while the stressed volume creates an elastic recoil pressure that is an important factor in the generation of blood flow and depends on the vascular compliance of a specific compartment. The reader is referred to Reference 25 for a comprehensive description of the blood volume distribution between different vascular districts, which includes assignment of compliances and unstressed volume.

2.1.6 | Cerebrospinal fluid model

The blood circulation model is coupled to a simple model of the cerebro-spinal cavity. This model, based on References 18,21, is characterized by a single compartment representing the cranial and spinal cavity with elastic behavior allowing for volume changes. Variations in cerebral blood volume produce fluctuations in intracranial pressure. Intracranial pressure is in turn used as external pressure for all cerebral compartments, that is, in one-dimensional vessels, 0D compartments of the microcirculation and Starling resistors.

2.1.7 | Cerebral autoregulation

Cerebral autoregulation is a mechanism which aims to maintain stable cerebral blood flow despite changes in arterial pressure. Three key mechanisms, the myogenic, metabolic and neurogenic, play a role in the cerebral autoregulation.

The myogenic process refers to the active behavior of the vasculature in response to changes in arterial blood pressure; changes in strain of the walls of the small arteries results in vasoconstriction or vasodilation, hence modifications in the resistance to blood flow. The metabolic response results from any local mismatch between supply and demand for oxygen while the neurogenic response is the least well understood since sympathetic activity has been proved to be the hardest both to interpret and to measure.[29] In this work, cerebral arterial circulation is controlled by a cerebral autoregulation model which acts on resistances and compliances of terminal arteries, arterioles and capillaries compartments in response to changes in cerebral blood flow. The action of myogenic regulation includes a static gain and first-order low-pass dynamics. An increase in cerebral blood flow causes vasoconstriction, with consequently decrease in compliance and increase in resistance of cerebral arterioles/capillaries. The regulatory response is modeled by a sigmoidal static relationship with upper and lower levels which account for limited vasodilation and vasoconstriction capacities.[20,22,23]

2.1.8 | Baroreflex control

The baroreceptor system is one of the major short-term pressure regulation mechanisms. Baroreceptors in carotid arteries in the neck and in the arch of the aorta are stimulated by stretch of the arterial wall due to alterations in arterial blood pressure, while low-pressure baroreceptors are activated by the right atrial pressure. Alterations in the arterial pressure and/or in the venous pressure affect the firing rates of afferent fibers; such rates are modeled via sigmoid functions that depend on arterial and venous pressure changes.[24,31,51] The averaged responses mediated by the sympathetic and parasympathetic systems are a combination of pressure changes. Baroreflex acts on heart rate, maximum value of elastance of the four cardiac chambers, arterial resistance (which comprises proximal resistance of 1D terminal arteries and resistance of arteriolar compartment of vascular beds for all vascular districts, except for the brain), and venous compliance and unstressed volume (i.e., the venous tone) of venules compartment of non-intracranial vascular beds and 1D veins. A detailed description of the model and how it is incorporated in the present global model can be found in References 24,25,31.

2.1.9 | Parametrization of the model

The parameters needed for the implementation of the global closed-loop model are defined in order to simulate a young healthy subject (aged 25 years old). Unless specified otherwise in this work, the parametrization is the same as the one reported in References 20,25. While Table A1 provides a summary of model equations and parameters, we refer the reader to the works in References 18–20,25 for more details about the model description, parameter selection, and validation of the baseline state.

2.2 | Hypertensive scenario

Pathophysiological studies have extensively investigated the remodeling and functional changes in hypertension. Here, we modify our model in order to reproduce main changes experienced by the cardiovascular system for the hypertensive condition. We focused on middle-aged (41–65 years[2]) untreated subject with mild to moderate hypertension (systolic pressure 130–159 mm Hg, diastolic pressure 85–99 mm Hg) and we adjusted the model parameters according to observations reported in the literature. Main modifications involve large arteries stiffness, peripheral resistance of small arteries and arterioles, decrease in capillary density, left ventricular hypertrophy of the heart and compliance of the venous system. We adopted the model representing the supine position, and therefore that effect of gravity was disregarded. Table 1 summarizes how the affected parameters change from normotensive to hypertensive parametrization.

   Large arteries alterations associated with hypertension may involve both structural and mechanical properties of arterial wall. Moreover, aging mainly affects large arteries by the arteriosclerosis process.[52,53] The remodeling due to aging and hypertension is not homogeneous along the aortic tree. Arteries can be subdivided into two types: elastic and muscular; the first group has relatively large diameters and are located close to the heart (thoracic aorta, common carotid artery, and aortic root), while muscular arteries are located at the periphery (femoral, brachial, and radial arteries). It has been observed that elastic arteries of hypertensive subjects are characterized by an increase in intima-media

TABLE 1 Hypertensive scenario parametrization.

Cardiovascular compartment	Parameter	Normotensive parameter	Hypertensive parameter
Elastic arteries	Radius	$r_0 = \overline{r_0}$	$r_0 = 1.1\overline{r_0}$
	Pulse wave velocity	$c_0 = \overline{c_0}$	$c_0 = 1.4\overline{c_0}$
	Viscoelasticity	$\Gamma = \overline{\Gamma}$	$\Gamma = 1.1\overline{\Gamma}$
Muscular arteries	Wall thickness over wall radius	$\frac{h_0}{r_0}$	$1.4\,\frac{h_0}{r_0}$
	Viscoelasticity	$\Gamma = \overline{\Gamma}$	$\Gamma = 1.4\overline{\Gamma}$
Small arteries, arterioles and capillaries	Arterial impedance	$R_{da} = \overline{R_{da}}$	$R_{da} = 1.4\overline{R_{da}}$
	Arterioles resistance	$R_{al} = \overline{R_{al}}$	$R_{al} = 1.4\overline{R_{al}}$
	Capillaries resistance	$R_{cp} = \overline{R_{cp}}$	$R_{cp} = 1.1\overline{R_{cp}}$
Left ventricle	Active elastance	$E_A = 2.75$ mm Hg/mL	$E_A = 3.57$ mm Hg/mL
	Passive elastance	$E_B = 0.12$ mm Hg/mL	$E_B = 0.156$ mm Hg/mL
Pulmonary circulation	Arterial resistance	$R_A = 0.04$ mm Hg/s/mL	$R_A = 0.056$ mm Hg/s/mL
Venous circulation	Venous compliance	111.0 mL/mm Hg	83.0 mL/mm Hg
Baroreflex control	Arterial level of activation	$\mu = 91.20$ mm Hg	$\mu = 124.63$ mm Hg
	Venous level of activation	$\delta = 4.21$ mm Hg	$\delta = 5.16$ mm Hg

Note: Changes between normotensive and hypertensive parameters. For 1D arteries and arterial microcirculation, the baseline parameter in normotensive state is indicated with overline while the variation in hypertensive parametrization is given with percentage with respect to the baseline. Parameter notation and reference equations can be found in Appendix A. Values provided for variables controlled by the baroreflex model (R_{da}, E_A and venous compliance) should be considered as setting point values. The actual value of these variables will change when controlled variables deviate from their setting point.

thickness and lumen enlargement.[54–56] On the other hand, muscular arteries are characterized by increased thickness but no change in lumen diameter; moreover, the elastic response is maintained despite hypertrophy of the arterial wall.[57] In view of this evidence, we divide the network of arteries into elastic (along the aortic branch) and muscular vessels. According to Reference 57, the ratio between wall thickness and internal radius increases by 40% in muscular peripheral arteries while it is not significantly changed in elastic arteries.[54] On the contrary, the elastic modulus increases by 45% in elastic arteries and remains unchanged in the other group. Radius of elastic arteries increases by 10% since it was proved that aortic root size increases with aging[58]; in order to maintain normal ratio between wall thickness and internal radius, the wall thickness increases proportionally. These modifications do not affect the stiffness $K(x)$. However, since we are interested in middle-aged hypertensive subjects, the intrinsic stiffness of elastic arteries is augmented due to the aging process. This physiological behavior is translated into the mathematical model in order to generate a 40% increase in pulse wave velocity. For muscular arteries we consider an augmented wall thickness for the evaluation of the stiffness $K(x)$ to match the carotid-femoral pulse wave velocity increase by 40%.

In this paper, we are considering a viscoelastic behavior of the vessels wall, which depends on Γ; this parameter describes the viscoelastic properties of the wall and it is proportional to the vessel wall thickness, as described in Equation (3). Therefore, in the hypertensive scenario, we increase Γ for both elastic and muscular arteries proportionally to the hypertension-related wall thickening.

Vasoconstriction, eutrophic remodeling with increased media-to-lumen ratio, decreased vasodilation reserve, and rarefaction characterize small resistance arteries in patients with essential hypertension.[56] According to the literature, the main site for structural elevation of resistance is the proximal part of the microcirculation; for this reason, R_{da} and R_{al} increase by 40% to account for a decrease in small vessel radii of about 7%–8% and an increase in blood viscosity.[56,59–61] On the other hand, the capillaries, that are crucially important for local flow distribution, are partly protected from pressure elevation by a raised resistance upstream. Resistance vessels ensure that the mean intra-capillary pressure remains within a tightly controlled range well below the arterial level for preservation of the structural integrity of the fragile capillary wall. Therefore, R_{cp} increases by only 10% in order to consider the reduction of capillary density that characterizes the aging process.[59,62]

Elevated systemic load induced by hypertension leads to left ventricular hypertrophy in the heart. Enlargement and thickening of the heart muscle of the left ventricle maintain the systolic wall stress at normal values despite increased load. Both active and passive elastance were increased by 30% to match literature data.[12]

Concerning the heart rate, there is no appreciable difference between the normo- and hypertensive patients. McEniery et al.[63] reported an heart rate of 69 ± 12 beats/min in an healthy group of 5648 patients and 70 ± 12 beats/min in an hypertensive group of 3420 subjects. Abdelhammed et al.[64] found that normal subjects (19 people) have an heart rate of 68 ± 12 beats/min while hypertensive patients at stage I of the disease (systolic blood pressure 140–159 mm Hg, diastolic blood pressure 90–99 mm Hg) with uncontrolled blood pressure (44 subjects) have an heart rate of 70.6 ± 10.6 beats/min. They also observed that heart rate tended to be higher in the pre-hypertensive group, but this difference was not statistically significant. For this reason, the same cardiac cycle duration (0.8 s) has been adopted for simulations of both the normotensive and hypertensive subjects.

As in the systemic circulation, the arterial pulmonary pressure and resistance increase in hypertension. Hence, the resistance of the arterial compartment of the pulmonary circulation was increased by 40%.[65,66] On the other hand, pulmonary compliance remains unchanged since it was observed that intrathoracic vascular compliance is comparable between normotensive and hypertensive patients.[67,68]

It has been observed that total intravascular volume is normal or decreased in hypertension.[65] In addition, human and animal studies revealed that vascular compliance is reduced.[67,69–74] In view of these considerations, we set up the same total blood volume in both normotensive and hypertensive subjects while venous compliance is reduced by 25%. Increased stiffness in 1D arteries leads to decreased total arterial compliance. Hence, the parameter for total arterial compliance, which includes both 1D arteries compliance and arterial microvasculature compliance, is reduced so that the arterial/arteriolar part of (0D) vascular beds is characterized by the same compliance of the normotensive case. For the assessment of the total effective vascular compliance, we perform a blood infusion test of 500 mL in 4 min in normotensive and hypertensive context, following the experimental procedure proposed in References 69,75. We refer the reader to Reference 25 for a complete discussion on how to perform this test, the mathematical modeling implications and a comparison with the existing literature in normotensive case.

Hypertension results in chronic adaptation of the cerebral circulation to higher levels of blood pressure, such that the autoregulated curve of cerebral blood flow is shifted to the right with respect to the setting point used for normotensive individuals.[76] This implies that, if blood pressure is lowered to a level that would be safe in nonhypertensive individuals, the brain would be more susceptible to hypoperfusion. This right shifting of the autoregulation curve, first described in animals model and then verified in a limited number of hypertensive individuals, has been attributed to the increase in vascular resistance induced by remodeling in cerebral vessels.[76] In our model, we reproduce the shift of this curve resetting the baseline values of arterial resistances and volumes to the hypertensive status determined by means of a simulation in the hypertensive scenario without the action of control mechanisms.

The same happens with the baroreceptors regulation. According to literature data,[77] the baroreceptor reflexes are reset towards a higher blood pressure level. Therefore, the baseline levels of activation for both high- and low-pressure baroreceptors are reset to the new hypertensive states, evaluated by means of a simulation in the hypertensive scenario without the action of regulatory mechanisms. Moreover, the baroreflex seems to operate with reduced sensitivity in hypertension; there is evidence that this occurs in sustained hypertensive patients and it is secondary to elevated blood pressure rather than playing a role in early stage of the disease.[77] Since we are considering a mild to moderate class of hypertensive subjects, we do not consider this aspect.

3 | NUMERICAL RESULTS

In this section, we introduce the computational results obtained with the presented model in normotensive and hypertensive subjects; we compare them with literature data in order to perform a detailed validation of model's outputs. The section focuses on large and small arteries, the heart and pulmonary circulation, total blood volume and vascular compliance, the venous system. Results were obtained using the numerical approach described in Section 2.1.1. In brief, we used a local time-stepping second-order path-conservative numerical scheme with a characteristic mesh length of 1 cm and a CFL number of CFL = 0.9. Simulations for the normo- and hypertensive states were run until a periodic state was reached, normally after 40 s. Mesh independence and periodicity were determined by verifying that results did not differ by more than 0.5% between two successive meshes and cardiac cycles, respectively. In the case of the infusion tests, injection of blood took place after the reference normo- and hypertensive periodic states were reached, while the final state at which variables were assessed regarded the new periodic state reached after the control mechanisms stabilized.

3.1 | Large and small arteries remodeling

Table 2 shows the main cardiovascular indexes linked to the arterial circulation; we refer to systolic, diastolic, mean and pulse pressure in brachial, carotid and aortic arteries, as well to pulse pressure indexes (augmentation index and pulse pressure amplification), pulse wave velocities and arterial compliance index. Computed values in normotensive and hypertensive subjects are compared with literature data. In the hypertensive scenario, systolic, diastolic and mean blood pressures values in brachial, carotid and aortic arteries well reproduce the pressure rise that was clinically observed in patients at stage I of the disease. Figure 2 compares the computed waveforms over a cardiac cycle along the aorta and major arteries of the lower limb in normotensive and hypertensive subjects. Cardiac-cycle averaged pressure values are reported for each analyzed artery above the corresponding plot in Figure 2; a comparable increase in mean arterial pressure can be observed for all observed locations in the arterial tree.

The assessment of arterial stiffening is performed by means of cardiovascular indexes usually adopted in the clinical practice. Table 2 reports augmented pressure, augmentation index, pulse pressure amplification, carotid-femoral and brachial-ankle pulse wave velocities (PWV) and total arterial compliance index. Details on how these index are computed can be found in the Appendix B. Augmented pressure, and in turn augmentation index, are increased in hypertensive scenario as a consequence of early return of the reflected waves. Computed augmentation index goes from 10.91% in normotensive subject to 17.91% in hypertension (Table 2). Pulse pressure amplification is reduced due to the aging process. Both computed PWV are increased in hypertensive scenario; their values are in line with literature data about young normotensive patients and elderly hypertensive subjects. As a consequence of increased arterial stiffness, arterial compliance is reduced. The hypertensive scenario yielded a significantly lower total arterial compliance index (0.55 mL/m^2/mm Hg vs. 0.97 mL/m^2/mm Hg in healthy condition, see Table 2).

For the local assessment of arteries stiffness, we consider two exemplary arteries, as usually done in the medical studies: the common carotid artery, as elastic artery, and the radial artery, as example of muscular artery. Figure 3 compares the pressure-diameter curves of these arteries with respect to literature data.[57,82] Comparing the computed pressure-diameter curve with respect to Reference 82, we can notice that the modeling pressure-area relationship, the so called tube law in Equation (2), is able to satisfactorily reproduce the physiological behavior of the vessel's wall

**TABLE 2** Cardiovascular indexes: comparison between normo- and hypertensive subjects.

Index	Normotensive		Hypertensive		References
	Value	**Ref. value**	**Value**	**Ref. value**	**References**
Brachial SBP (mm Hg)	111.52	115 ± 11	162.98	153 ± 22	54
Brachial DBP (mm Hg)	73.14	71 ± 7	90.41	99 ± 10	54
Brachial MBP (mm Hg)	89.74	86 ± 8	124.28	119 ± 12	54
Brachial PP (mm Hg)	38.38	38 ± 2.8	71.24	56.4 ± 14.7	78
Carotid SBP (mm Hg)	109.46	118 ± 14	162.84	166 ± 24	54
Carotid DBP (mm Hg)	73.59	70 ± 7	91.14	95 ± 12	54
Carotid PP (mm Hg)	35.96	48 ± 15	71.70	71 ± 24	54
Aortic SBP (mm Hg)	108.15	108 ± 12	161.72	140 ± 17	63
Aortic DBP (mm Hg)	74.05	75 ± 8	91.61	88 ± 11	63
Aortic PP (mm Hg)	34.10	33 ± 10	70.10	52 ± 17	63
Augmented P (mm Hg)	3.72	7 ± 7	12.56	16 ± 10	63
Augmentation index (%)	10.91	18 ± 18	17.91	28 ± 14	63
PP$_{Amplification}$	1.12	1.44 ± 0.25	1.03	1.30 ± 0.2	63
cfPWV (m/s)	9.27	8.5 ± 1.5	14.21	11.8 ± 2.7	79
baPWV (m/s)	11.46	14.84 ± 3.4	16.05	16.7 ± 3.6	80,81
C_a index (mL/mm Hg/m^2)	0.97	1.08 ± 0.25	0.55	0.61 ± 0.19	64

Note: Details on how to evaluate these indexes can be found in the Appendix B.

Abbreviations: Augmented P, augmented pressure; baPWV, brachial-ankle pulse wave velocity; C_a index, total arterial compliance index[64]; cfPWV, carotid-femoral pulse wave velocity; MBP, mean blood pressure; PP, pulse pressure; (S/D)BP, systolic/diastolic blood pressure.
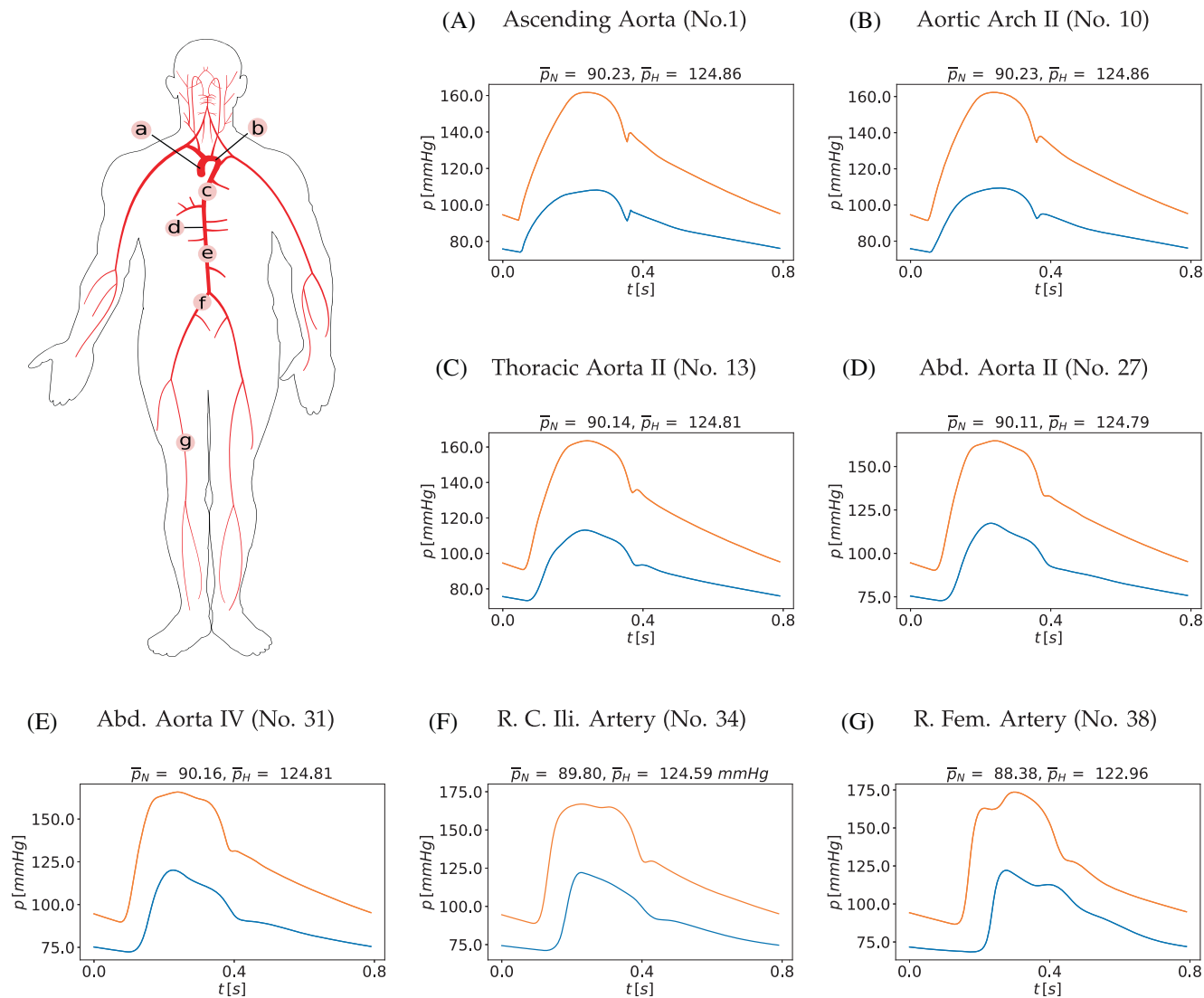
FIGURE 2 Computed blood pressure in the aortic tree at different locations (A–G) in normotensive (blue line) and in hypertensive (orange line) states. Cardiac-cycle averaged values are denoted by $\overline{p}_N$ (normotensive) and $\overline{p}_H$ (hypertensive).
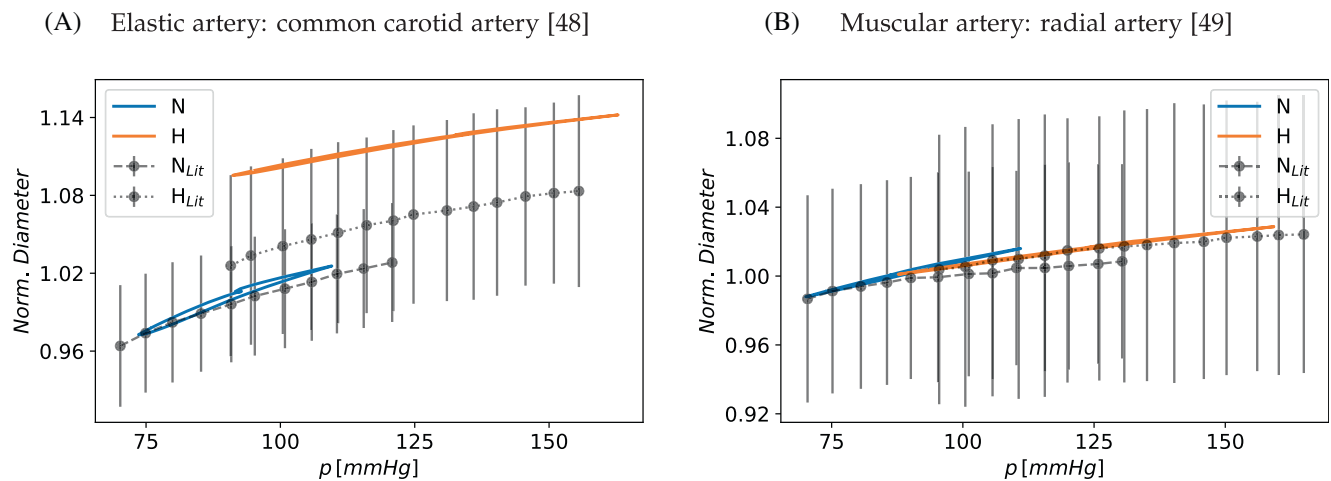
**FIGURE 3** Computed diameter–pressure curve in right common carotid artery and in right radial artery in normotensive (N) and hypertensive (H) subjects. Computational results are compared to literature data in References 57,82 (mean $\pm$ SEM) for both normotensive (N_{Lit}) and hypertensive (H_{Lit}) states. Diameter is normalized with respect to the average value over a cardiac cycle.

deformation in both normotensive and hypertensive subjects. The lumen enlargement is more pronounced in the elastic artery, while in the muscular artery the area is slightly increased, as observed in the experimental data.

The increase in pulse pressure that characterizes the 1D arterial vessels is reflected also in the arterioles' compartments but it is attenuated in the capillaries compartments. Figure 4 shows the pressure waveforms along the vascular system of the right arm: from the radial artery to capillary beds. In this figure it is easy to observe that the arrival time of the arterial pressure wave to all considered microvascular compartments changes as expected, with an anticipation of the late diastole foot in hypertension with respect to the localization of that waveform feature in results concerning the normotensive scenario. Table 3 reports computed pressure at different arterial vascular levels. We consider all the vascular beds of the model and evaluate the pressure variations in the arterial compartments between healthy and pathological cases; data about mean pressure over a cardiac cycle are presented as mean $\pm$ standard deviation of all vascular beds. It can be observed that the main sites of elevation of blood pressure are 1D arteries and arterioles.

Pulsatility and resistive indexes (PI and RI) are clinically used for the determination of end-organ damage. Pulsatility index is defined as the difference between the peak systolic and minimum diastolic flow rate, divided by the mean flow rate over a cardiac cycle, or equivalently, as the difference between the peak systolic and minimum diastolic flow velocity, divided by the mean velocity over a cardiac cycle. In the 1D arterial network, PI ranges between 0.71 and 7.3 and in general it is lower in the hypertensive scenario with respect to the normotensive one. The percentage difference is -4.64 ± 16.9, evaluated as mean and standard deviation over the complete arterial 1D network. However, some 1D arteries present higher pulsatility indexes: these include mainly arteries of the abdominal region, such as abdominal, gastric, hepatic arteries, as well as cerebral arteries. Table 4 reports computed pulsatility and resistive indexes in renal and cerebral arteries compared to literature ranges. In our computational results, there are no significant changes between computed PI in normotensive and hypertensive subjects. In the vascular bed of the splanchnic circulation, computed PI from the flow waveform of the arterioles' and capillaries' compartments increases by about 13%, while in the vascular bed of the renal circulation PI increases by about 6.3%. Computed indexes are in line with values reported in the literature; however, computational results do not reproduce the significant rise in PI of renal arteries observed in clinical measurements. Concerning the cerebral circulation, previous works mainly focused on carotid and middle cerebral arteries to study the haemodynamic changes associated with hypertension. From computational results (Table 4), we can observe that in these arteries PI tends to decrease from normotensive condition to hypertension, even if their values are comparable to literature measurements. A different behavior can be observed at the level of 0D arterioles/
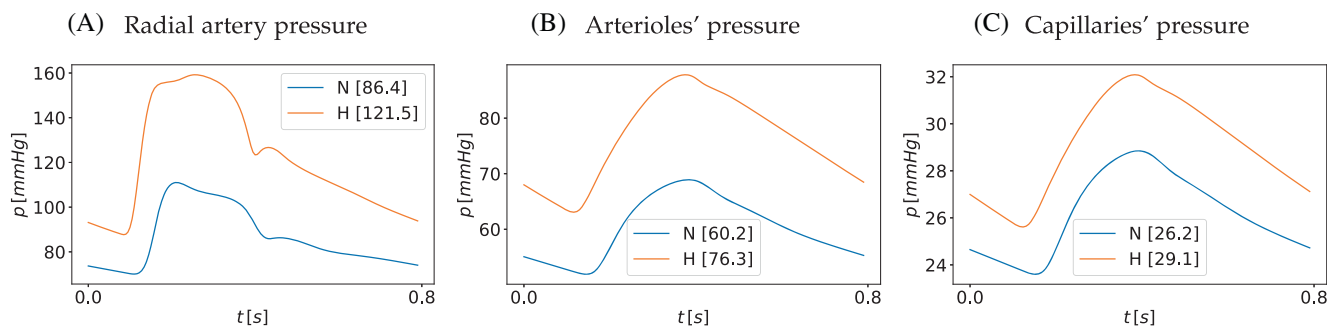
FIGURE 4 Computed pressure variations along the vascular system of the right arm, specifically of the right radial artery and its terminal arteriolar and capillary compartments. *N*: normotensive subject; *H*: hypertensive subject. Cardiac-cycle averaged values are reported in brackets.

TABLE 3 Arterial pressures: pressure variations in the arterial compartments between healthy and hypertensive cases; data about mean pressure over a cardiac cycle are presented as mean $\pm$ standard deviation of all vascular beds.

Index	Normotensive	Hypertensive
Terminal arteries pressure (mm Hg)	88 ± 1.44	122.78 ± 1.44
Arterioles pressure (mm Hg)	74.77 ± 6.66	99.40 ± 11.35
Capillary pressure (mm Hg)	29.99 ± 2.62	34.23 ± 3.42
Capillary pulse pressure (mm Hg)	5.24 ± 2.48	6.47 ± 2.82

TABLE 4 Pulsatility and resistive indexes in renal and cerebral circulations: comparison between normo- and hypertensive subjects.

	Normotensive		Hypertensive		
Index	Value	Ref. value	Value	Ref. value	References
Renal circulation					
PI—renal arteries	1.52	1.19 (0.93–1.25)	1.53	1.65 (1.31–1.86)	83
RI—renal arteries	0.70	0.67 (0.64–0.70)	0.75	0.76 (0.69–0.81)	83
Cerebral circulation					
PI—ICAs	1.02	0.84 ± 0.11	0.84	0.88 ± 0.19	84
RI—ICAs	0.58	0.79 ± 0.12	0.54	0.81 ± 0.12	84
PI—MCAs	0.74	0.54 ± 0.05	0.69	0.55 ± 0.07	84
RI—MCAs	0.48	0.52 ± 0.05	0.49	0.52 ± 0.05	84

Note: Arteries under consideration are renal arteries, internal carotid arteries (ICAs), middle cerebral arteries (MCAs). Computed values are mean values between right and left arteries. Details on how to evaluate these indexes can be found in the Appendix B.

small arteries and capillaries. In cerebral vascular beds, PI computed on flow rate waveforms increases by about 25%–29% in both arterioles and capillaries from normotensive to hypertensive condition.

3.2 | The heart

Table 5 presents some of the main cardiac indexes. The cardiac index (the ratio between cardiac output and body surface area) is comparable between normotensive and hypertensive state, as well as the stroke index, evaluated as stroke volume over body surface area. We stress that the same body surface area of 1.92 m^2 has been adopted in the healthy and pathological subjects for the evaluation of cardiac and stroke indexes; Abdelhammed et al.[64] reported 1.93 ± 0.25 m^2 in an healthy group while 1.91 ± 0.20 m^2 in an hypertensive group at stage I of the disease. Considering arterial elastance, E_a, and left ventricle elastance, E_{es}, Table 5 shows that they increase by the same ratio in the hypertensive group compared to the normotensive one, meaning that left ventricular-arterial coupling (E_a/E_{es}) is similar in both groups. Computational results in Table 5 stress also the behavior of right part of the heart, that is not immune to the effects of systemic hypertension. The right-heart pressures among the hypertensive patients increase significantly with respect to the values in the normotensive controls. In the same way, pulmonary arterial pressure increases in hypertensive patients with respect to values observed in the normotensive scenario: mean, systolic and diastolic pressure in the arterial pulmonary compartment are reported and compared to literature data from Reference 85.

Figure 5 shows the pressure-volume relationship in the left and right ventricles for normotensive and hypertensive subjects. In the left frame, which is referred to left ventricle, it can be observed the right shift of the curve as effect of left ventricle hypertrophy. Even if the parameters that characterize the model of the right ventricle are not modified in the hypertensive scenario, our computational results (Figure 5, right frame) display a hypertrophic behavior as a consequence of left ventricle hypertrophy and increased pulmonary arterial resistance.

3.3 | Total blood volume and vascular compliance

Total effective vascular compliance (TEVC) was computationally estimated in our model by means of an infusion test, as described in Reference 25. In short, a 500 mL blood infusion was simulated by adding a flow source at the level of the left atrium, starting from a periodic solution for both normo- and hypertensive model setups. The infusion started at 80 s and ended at 320 s. The infusion caused a deviation of arterial and venous pressure from setting point values, which in turn resulted in baroreflex control acting on model parameters to control these variables. After the transient caused by the infusion and baroreflex action, the new periodic state was reached in about 40 s and the simulations were stopped at 400 s. Main cardiovascular indexes were computed after the periodic state was reached. Figure 6 (left) shows the computed linear relation between volume and right atrial pressure modifications due to the rapid infusion of blood. The value of TEVC is expressed in mL/mm Hg and then normalized to the body weight, considered to be 75 kg in the

TABLE 5 Cardiac and pulmonary indexes: comparison between normo- and hypertensive subject.

Index	Normotensive		Hypertensive		References
	Value	Ref. value	Value	Ref. value	
HR (beats/min)	75	75 ± 12	75	77 ± 9	85
CI (L/min/m^2)	2.76	2.9 ± 0.8	2.97	3.1 ± 0.8	86
SI (mL/m^2)	37.48	43 ± 9	40.22	45 ± 11	86
E_a (mm Hg/mL)	1.32	1.52 ± 0.1	1.83	1.8 ± 0.17	87
E_{es} (mm Hg/mL)	2.14	2.03 ± 0.2	2.80	2.43 ± 0.2	87
E_a/E_{es}	0.61	0.77 ± 0.04	0.65	0.73 ± 0.06	87
LV_{max} (mL)	116.25	150 ± 67	127.59		38
LV_{EF} (−)	0.62	0.68 ± 0.12	0.61		38
RV_{max} (mL)	126.96	173 ± 95	149.15		38
RV_{EF} (−)	0.56	0.57 ± 0.10	0.51	0.59 ± 7	38,85
max. $\frac{dP_{LV}}{dt}$ (mm Hg/s)	1505.59	1915 ± 410	2139.55		38
min. $\frac{dP_{LV}}{dt}$ (mm Hg/s)	−2505.36	-2296 ± 530	−4253.05		38
max. $\frac{dP_{RV}}{dt}$ (mm Hg/s)	262.08	248 ± 25	322.60		38
min. $\frac{dP_{RV}}{dt}$ (mm Hg/s)	−306.79	-232	−459.90		38
RV-SP (mm Hg)	25.31	22 ± 6	34.57	27 ± 5	85
RV-EDP (mm Hg)	2.42	3 ± 2	3.36	5 ± 2	85
MPAP (mm Hg)	16.14	12 ± 3	21.97	17 ± 5	85
SPAP (mm Hg)	24.68	20 ± 6	33.87	26 ± 6	85
DPAP (mm Hg)	10.61	8 ± 2	14.22	11 ± 5	85

Note: Details on how to evaluate these indexes can be found in the Appendix B.

Abbreviations: CI, cardiac index; E_a, arterial elastance; E_a/E_{es}, arterial-ventricular coupling index; E_{es}, left ventricle elastance; HR, heart rate; LV/RV$_{EF}$, ejection fraction of ventricle; LV/RV$_{max}$, maximum volume of ventricle; M/S/D PAP, mean/systolic/diastolic pulmonary artery pressure; max/min $\frac{dP}{dt}$, maximum/minimum pressure rate; RV-EDP, right ventricle end-diastolic pressure; RV-SP, right ventricle systolic pressure; SI, stroke index.
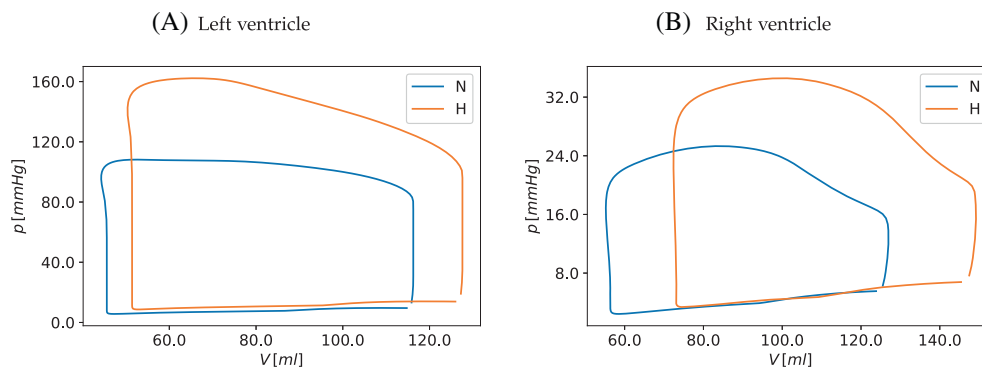

(A) Left ventricle (B) Right ventricle

FIGURE 5 Computed volume–pressure relationship of the left and right cardiac ventricles. Comparison between normotensive subject (*N*) and hypertensive patient (*H*).

normotensive state and 85 kg in the hypertensive subject. We consider the same percentage increase in body weight between normo- and hypertensive groups reported by London et al.[69] Computational results show that TEVC is significantly reduced in hypertensive subjects (2.02 vs. 2.82 mL/mm Hg/kg in normotensive scenario).

Figure 6 (right) shows the percentage variation in main haemodynamic parameters before and after expansion. Computed results are compared to Reference 69. We can observe that cardiac output and cardiopulmonary blood volume increases with a similar percentage between normotensive and hypertensive patients, proving that the

cardiopulmonary capacity of accommodating blood volume remains comparable between normo- and hypertensive subjects. Heart rate decreases in normotensive case, while it increases in hypertension; however, changes in heart rate are not significant.

The decreased venous compliance produces a redistribution of blood volume; since total blood volume is normal or reduced and there is no decrease in the compliance of the cardiopulmonary circulation,[67,73,75] this results in a shift of blood to the central circulation (heart and lungs). Figure 7 shows the blood volume distribution in the main districts of the circulation: arterial blood (1D arteries, small arteries and arterioles), capillaries, venous blood (venules, small veins and 1D veins), heart and pulmonary circulation. It can be observed that in the hypertensive case, the arterial and capillaries percentages of blood volume are comparable to the normotensive state, but there is a slight increase in heart and pulmonary circulation amount of blood ($+3\%$), matched by a small decrease in venous blood.

3.4 | The venous system

Pressure, flow and PIs of some one-dimensional veins are compared between hypertensive and normotensive scenarios. Figure 8 shows the computed pressure waveforms in selected veins at different locations. One can observe that venous pressure increases by about 20% in all selected veins. The venous pulse pressure increases in the hypertensive scenario with respect to that obtained the normotensive state. In the inferior vena cava, it is 2.15 mm Hg in the normotensive
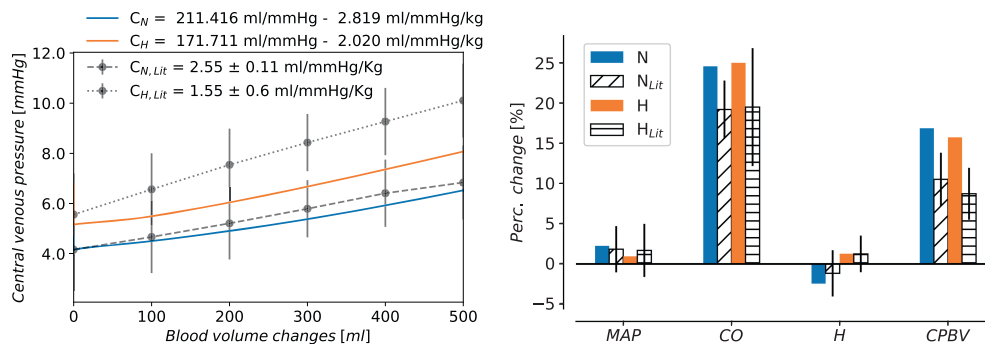
FIGURE 6 Left frame: computed total effective vascular compliance by means of an infusion test of 500 mL of blood in 4 min. Changes in mean central venous pressure are plotted against changes in total blood volume and the inverse of the slope of their linear relationship is the value of the effective compliance. Computed results are compared to literature data reported in Reference 69. Right frame: Changes in haemodynamic parameters before and after expansion for normo- and hypertensive scenarios. Computed results are compared to literature data from Reference 69. Parameters under consideration are MAP, mean arterial pressure; CO, cardiac output; H, heart rate; CPBV, cardiopulmonary blood volume.
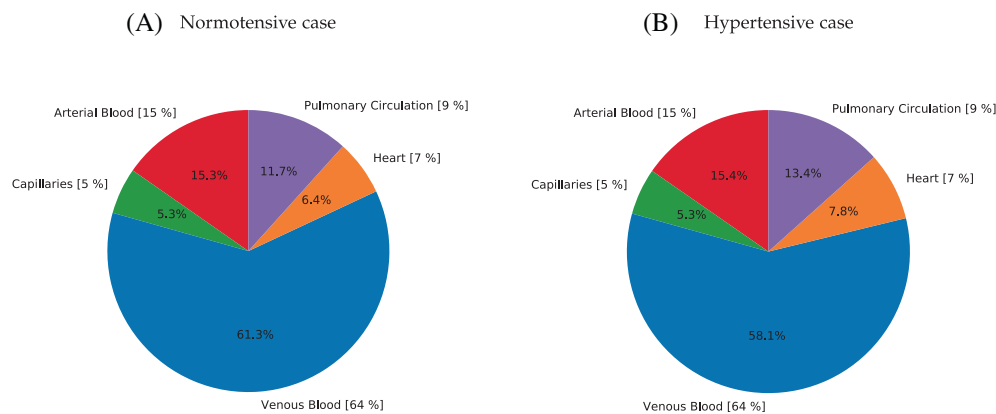
FIGURE 7 Computational blood volume distribution in normotensive and hypertensive subjects. Arterial blood: 1D arteries and arterioles' compartments. Venous blood: 1D veins and venules' compartments. Value in brackets refers to literature blood volume distribution in Reference 5.
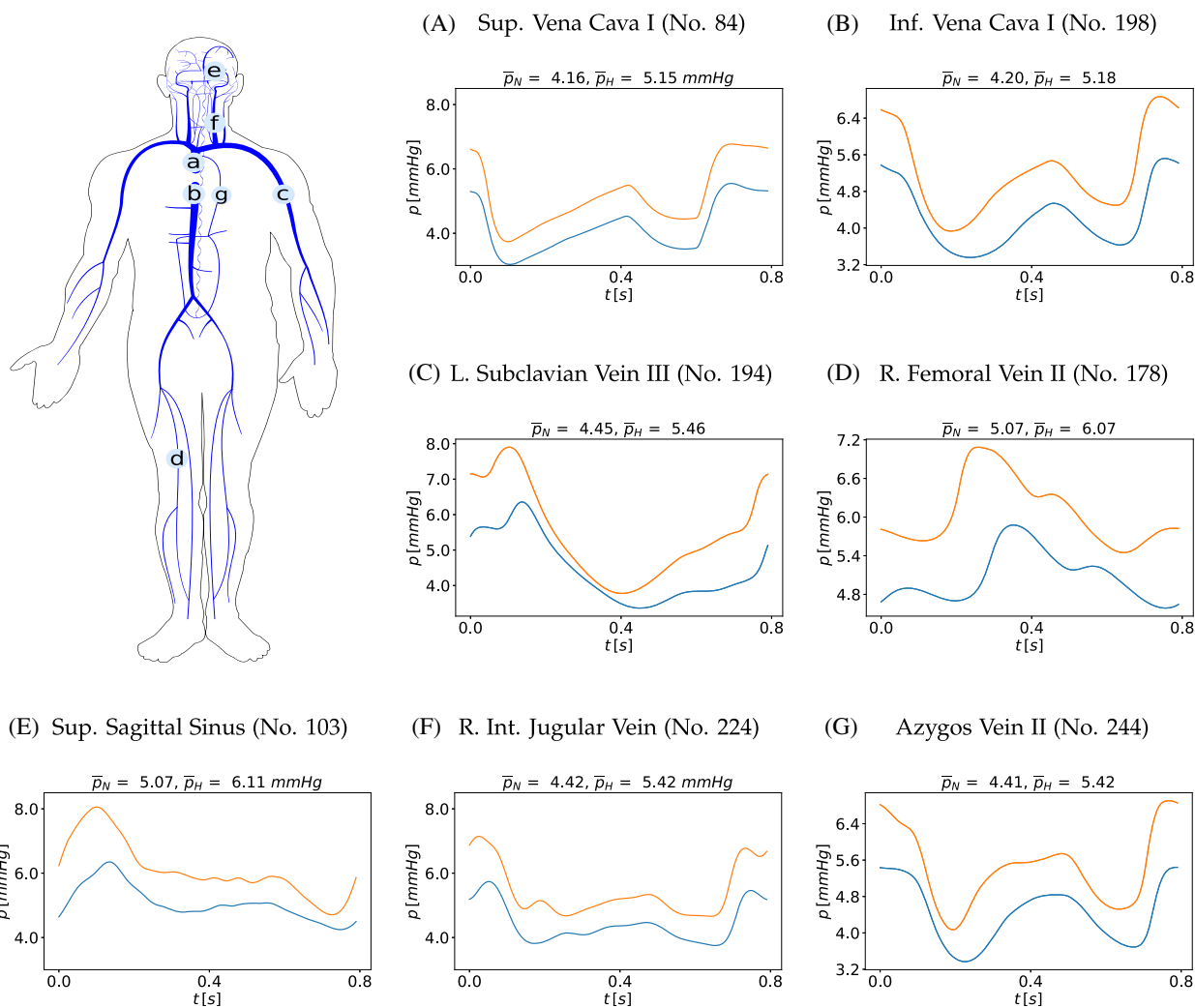
FIGURE 8 Computed blood pressure in selected veins at different locations (A–G) in normotensive (blue line) and in hypertensive (orange line) state. Cardiac-cycle averaged values are denoted by $\bar{p}_N$ (normotensive) and $\bar{p}_H$ (hypertensive).
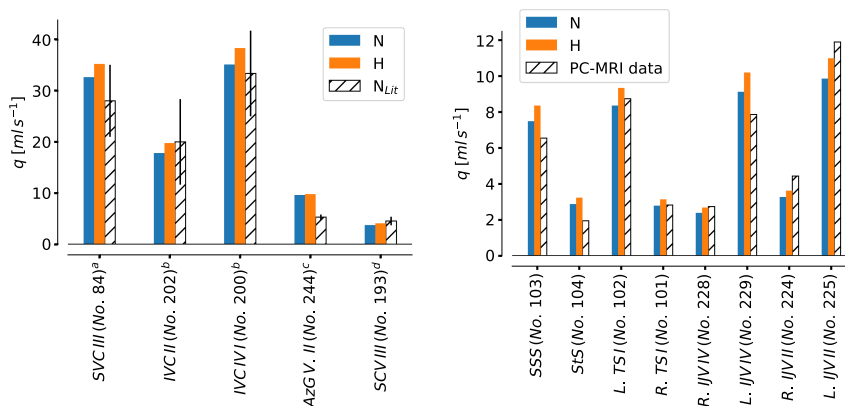
FIGURE 9 Blood flow distribution in selected systemic veins (left frame) and in head and neck veins. Computational results obtained in the hypertensive scenario are compared with computational data of the healthy subject and with literature data (average and standard deviation) or MRI flow quantification data.[19] Literature and MRI data regard normotensive subjects. Left frame: Mean flow rate in systemic veins. SVC, superior vena cava; IVC, inferior vena cava; AzG V., azygos vein; SCV, subclavian vein. Literature: [a]Murgo et al.[88]; [b]Wolf et al.[89]; [c]Zitnik et al.[90]; [d]Cheng et al.[91] Right frame: Mean flow rate in head and neck veins. SSS, superior sagittal sinus; StS, straight sinus; TS, transverse sinus; IJV, internal jugular vein.

case while 2.94 mm Hg in the hypertensive scenario (percentage difference of 36.13%). In dural sinuses, the change is more significant: in the superior sagittal sinus, venous pulse pressure increases from 2.10 mm Hg in normotensive subject to 3.35 mm Hg in hypertensive condition (percentage difference of 59.03%).

Concerning flow rate, Figure 9 shows the computed mean flow rate in selected systemic veins and in some head and neck veins. Computational results obtained in the hypertensive scenario are compared with computational results of the normotensive case, as well as with literature data or MRI flow quantification data of normotensive patients. In systemic veins, average flow rate is slightly increased (up to 10%) in hypertension with respect to values obtained in the normotensive subject. The same can be observed in head and neck veins, wherein average flow rate increases by 10%–13% with respect to what measured in veins of normotensive subject. The PI, evaluated from the flow waveform, also increases by about 30% along the entire venous network.

4 | DISCUSSION

4.1 | Modeling assumptions: a global mathematical model for studying hypertension

This paper describes how a global closed-loop model of the entire human circulation is parametrized in order to represent the hypertensive condition in middle-aged subjects. As already said, the baseline model was previously presented and validated with respect to all of its components.[18–20,25] Here, rather than constructing an ad-hoc model for the study of hypertension, we adapted our existing model to this condition, so that the different components of the model are available for further studies under hypertensive conditions. With this goal in mind, arteries and veins were still described by means of one-dimensional viscoelastic models even if the effect of viscoelasticity is negligible in hypertension and the venous system is less affected by this condition. Moreover, since we work with a global closed-loop model, all the main cardiovascular compartments were considered, independently of their effect and/or importance in arterial hypertension. In fact cerebrospinal fluid dynamics plays a very little role in hypertension, but its description with the model proposed in Reference 20 is kept in order to maintain the level of detail by which our model describes cerebral circulation, with intracranial pressure acting on the cerebral vasculature. The same approach is considered for the regulatory mechanisms included in the original model. In this work, we refer to two short-term regulatory systems. The first one is the cerebral autoregulation, which works on resistances and compliances of cerebral arterial vasculature, and was introduced in Reference 20. The second one is the baroreflex control, presented in Reference 25. Both mechanisms physiologically act in the range of minutes and they are short-term responses to rapid deviations from the baseline status. Here we are considering their resetting in the hypertensive condition. This means that, for results reported for baseline and hypertensive conditions, short-term regulation mechanisms are working at their setting points and thus not altering the state of the model. The only situation in which these control mechanisms are active is during the infusion tests presented in Section 3.3. This test affects the baroreflex model significantly and, as pointed out in Reference 25, baroreflex action on the cardiovascular system is essential for the estimation of the total effective vascular compliance. Mimicking the clinical practice, in this work we estimate total effective vascular compliance by means of a rapid infusion of blood which causes a deviation from the baseline condition, activating the baroreflex control which in turn acts on cardiovascular properties such as heart properties, peripheral resistance and venous tone. Not including a working baroreflex model would not allow us to correctly reproduce the state induced by the infusion test, as extensively discussed in Reference 25.

4.2 | Large and small arteries remodeling

4.2.1 | A brief review on large arteries remodeling

Over the last decades non-invasive and invasive techniques allowed a better quantification of vascular changes in hypertensive humans and experimental animals. Large arteries undergo outward hypertrophic remodeling (increase wall thickness with limited changes in vessel's radius) and increased stiffness with aging and hypertension. In elderly patients, stiffening of central large (thoracic aorta, carotid) arteries is associated with increased aortic diameter and wall thickness, elastic fragmentation and calcification, as well as elevated collagen content. Even if age and hypertension both alter the structure of arterial wall and stiffness, the anatomical and functional changes are not the same; structural

modifications in hypertension are accelerated with respect to age-related changes. Increased stiffness in hypertension is associated to hypertrophy of arterial wall and changes in the extracellular matrix, mainly an increase in collagen.[92] Currently, increased blood pressure is considered the major determinant of arterial stiffness changes in hypertension.[68,73,92]

High blood pressure increases circumferential wall stress unless the change in pressure is matched by a proportional variation in vessel's radius or thickness. According to the Laplace's equation, the circumferential wall stress σ is proportional to radius r, pressure p, and inversely proportional to thickness h:

$$\sigma = \frac{pr}{h}. \tag{5}$$

The elevated circumferential stress is the fundamental trigger for the adaptive response of the vessel wall. Wall thickening results from both cellular growth and synthesis of new extracellular material. All these changes alter the biomechanical properties of the arterial wall, and therefore wall-material stiffness, a parameter usually evaluated from the determination of incremental elastic modulus. For the evaluation of arterial structural changes in subjects with clinical hypertension, two different arteries have been widely studied: the common carotid and the radial artery. The latter is composed almost exclusively of vascular smooth muscle and serves as a model of a peripheral muscular artery, while the first one represents a central musculo-elastic artery. Laurent et al.[57] performed the first non-invasive study for the determination of the elastic characteristics of radial artery wall material in hypertensive patients. It was observed that the intima-media thickening compensates for the rise in blood pressure (lumen diameter is not enlarged), and circumferential wall stress is maintained within normal ranges.[56] Moreover, elastic response of the radial artery is maintained despite hypertrophy of the arterial wall. The authors concluded that at the site of distal, muscular, medium-size arteries, thanks to their hypertrophy, normal compliance is maintained despite the increase in intravascular pressure through the normalization of the Young's elastic modulus (the slope of the stress–strain relationship of vascular wall). This means that in these arteries any increase in stiffness in hypertensive subjects always returns to the normal range when pressure is reduced to the normal range. Furthermore, muscular arteries dilate in hypertensive subjects such that their compliance (absolute volume change with change in pressure) may appear to be normal or even increased.[57,93–95] At the site of hypertensive proximal elastic arteries, the intima-media thickening is insufficient to compensate for both the enlargement of internal diameter and the rise in blood pressure: circumferential wall stress is significantly increased compared to the one observed in normotensive subjects. The evaluation of the Young's elastic modulus of the common carotid artery[54] revealed that it is increased only in younger hypertensive patients, while in middle-aged and older patients, the mechanical properties of the carotid arterial wall material are unchanged. In Reference 82, the compliance of the carotid artery was determined in hypertensive patients and compared to age and sex-matched normotensive subjects. It was shown that compliance decreases as blood pressure increases; moreover, evaluation of compliance at the same blood pressure level revealed that it is not significantly different between hyper- and normotensive patients after adjustment for age, but it decreases with aging. This suggested that the decreased compliance in large elastic arteries in hypertensive subjects is due primarily to the increased distending pressure and that age-independent structural modifications of the arterial wall play only a minor role.[82] In this case, the stiffness results in increased pulse-wave velocity and alterations of amplitude and timing of wave reflections and thus causes a disproportionate increase in systolic and pulse pressure.[96]

4.2.2 | Assessment of arterial stiffening by means of pulse wave velocity, augmentation and arterial compliance indexes

Large artery stiffening is the most important pathophysiological determinant of hypertension and age-dependent increase in pulse pressure. As the wave travels away from the heart towards the periphery, the systolic peak pressure increases according to physiological patterns. $PP_{Amplification}$ is an index representing the disparity between central and peripheral pressure and is calculated as the ratio between brachial and aortic pulse pressure. As reported in the literature,[63] this index is reduced in the hypertensive scenario (Table 2); one of the most determining factors of the central-to-peripheral pressure gradient is aging process. The measurement of pulse wave velocity is generally accepted as the most simple, non-invasive, robust, and reproducible method with which to determine regional arterial stiffness.[56] Pulse wave velocity (PWV) is a measure of the speed at which the pressure waveform propagates along a segment of the arterial tree; the stiffer the vessel, the faster the wave travels. Carotid-femoral PWV (cfPWV) is evaluated as the distance between carotid and femoral artery divided by the transit time of the wave (evaluated with the foot-to-foot
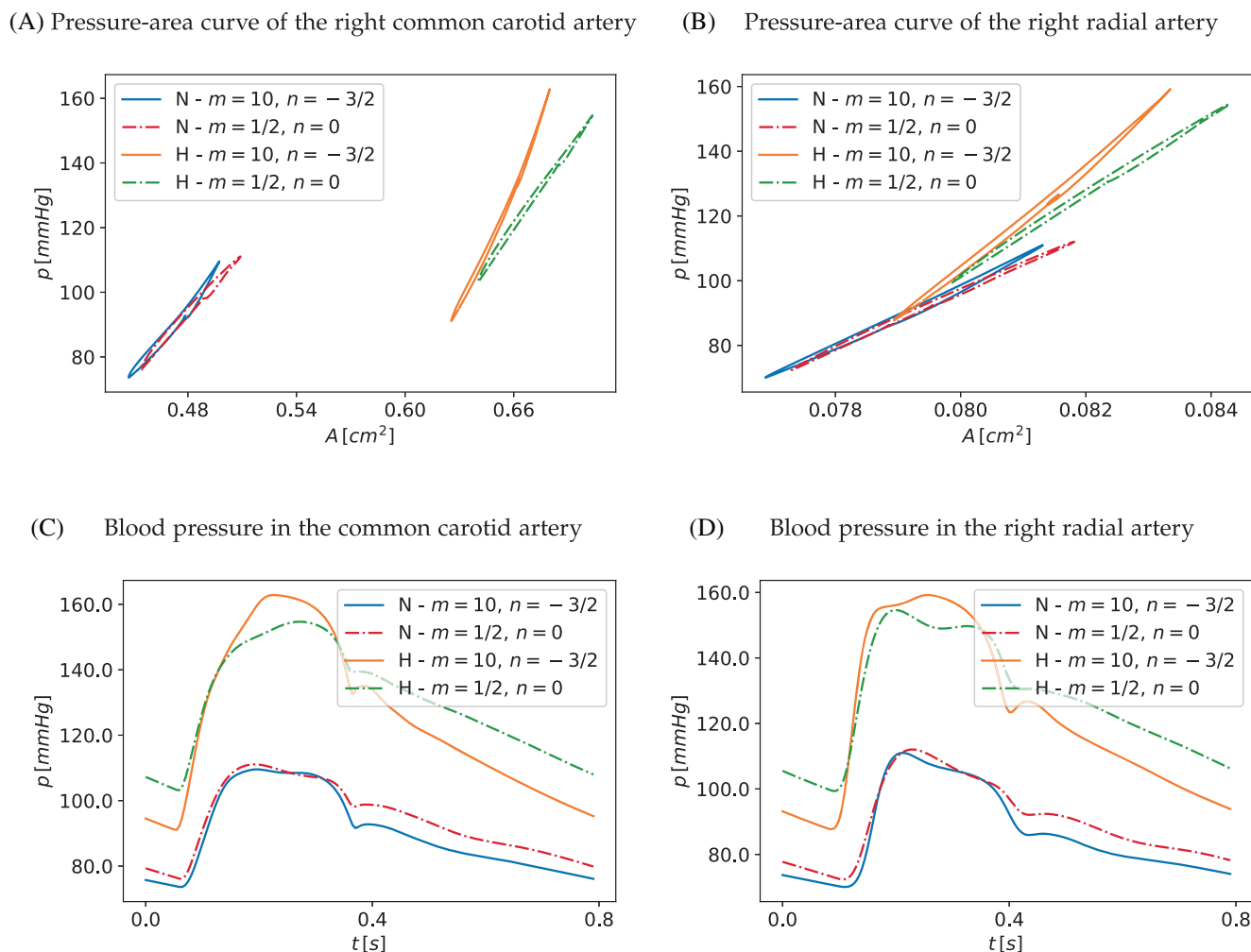
method). A cfPWV > 10 m/s is considered a conservative estimate of significant alterations of aortic function in middle-aged hypertensive patients.[2] The pulse wave velocity can be measured also at the brachial-ankle level, considering the brachial and the tibial arteries.[80,97] Both computed PWV are in line with literature data about young normotensive patients and elderly hypertensive subjects (Table 2). Augmentation pressure (Augmented P) is calculated as the difference between the second and first systolic peaks of aortic pressure, and augmentation index is calculated as augmentation pressure expressed as a percentage of the pulse pressure.[63] Augmentation index has been proposed as a measure of wave reflection; arterial stiffening increases the pulse wave velocity and hence causes an early return of the reflected wave[98]; computed augmentation index goes from 10.91% in normotensive subject to 17.91% in hypertension (Table 2). As a consequence of increased arterial stiffness, arterial compliance is reduced. Total arterial compliance index is evaluated as the ratio between stroke index and pulse pressure, as suggested in References 64,99, and compared to clinical data from Reference 64. The hypertensive scenario yielded a significantly lower total arterial compliance index (0.55 mL/m^2/mm Hg vs. 0.97 mL/m^2/mm Hg in healthy condition, see Table 2). Abdelhammed et al.[64] found that total arterial compliance index is lower in hypertensive patients at stage I and II of the disease, in both controlled and uncontrolled subjects; moreover, they stressed the correlation between this index and age.

4.2.3 | Computational pressure-area relationship of large arteries

Figure 3 compares the pressure–diameter curves of two exemplary arteries with respect to literature data.[57,82] In case of common carotid artery, we are considering a 10% enlargement of vessel's diameter, according to data in Reference 54. Comparing the computed pressure–diameter curve with respect to Reference 82, computational results for the hypertensive subject are at the limit of the physiological range; this is probably due to the fact that in Reference 82 middle-aged matched normotensive and hypertensive patients (50 ± 5 and 51 ± 3 years old, respectively) were compared. As stressed by Farasat et al.,[58] age accounts for dilation of large arteries, rather than hypertension; for adjustment with age, differences between aortic diameter of normotensive and hypertensive patients were not observed. In view of these considerations, since we are considering two groups of normotensive and hypertensive patients at different age, we believe that it is reasonable to observe a higher increase in diameter with respect to Reference 82. Anyway, we can notice that the lumen enlargement is more pronounced in the elastic artery, while in the muscular artery the area is slightly increased, as observed in the experimental data. Moreover, the modeling pressure-area relationship, the so called tube law in Equation (2), is able to satisfactorily reproduce the physiological behavior of the vessel's wall deformation. As previously said, Equation (2) depends on m and n, two experimental parameters that are usually taken $m > 0$ and n in the range $[-2, 0]$. The choice of $m = 1/2$ and $n = 0$ results in a tube law that does not reproduce the stiffening in the high blood pressure range; therefore, in this work we set $m = 10$, $n = -3/2$ in order to simulate a more realistic and physiological behavior. A similar choice for $m > 1$ was adopted in References 27,38,100. To stress the effect of this choice, we compare in Figure 10 the computed pressure-area curve and the computed pressure waveforms when $m = 1/2$, $n = 0$ (classical choice) and when $m = 10$, $n = -3/2$ obtained from simulations in normotensive and hypertensive conditions. In the normotensive case, both choices give comparable results; the differences are more evident in the hypertensive results. For $m = 10$, $n = -3/2$ one can see how the stiffening behavior results in higher pulse amplitude. In Figure 10C,D, arterial pressure curves over a cardiac cycle obtained with the two parametrizations of the tube law are displayed. The mean arterial pressure values are not significantly different: in hypertensive cases, radial artery mean pressure is 90.1 mm Hg when $m = 1/2$, $n = 0$, while it is 93.9 mm Hg when $m = 10$, $n = -3/2$ (percentage difference of 4%). On the contrary, pulse pressure is significantly affected: from 55.27 to 71.52 mm Hg in the radial artery of hypertensive scenario (percentage difference of 29.4%). If we consider the hypertensive scenario without imposing the stiffening of large arteries changing $K(x)$ in Equation (2), but simply a stiffer pressure-area relation given by $m = 10$, $n = -3/2$, the results reveal that this would be enough to match what is observed in hypertension. In fact, mean aortic pressure is 121.16 mm Hg, while systolic and diastolic pressures are 150.43 and 93.24 mm Hg, respectively. Pulse pressure at the aortic level is 57.19 mm Hg while at the brachial level it is 60.58 mm Hg.

4.2.4 | The arterioles and capillaries compartments

Computational results reveal that the main sites of elevation of blood pressure are 1D arteries and arterioles. Structural changes of small resistance arteries in patients with essential hypertension are usually a consequence of inward

(A) Pressure-area curve of the right common carotid artery

(B) Pressure-area curve of the right radial artery

(C) Blood pressure in the common carotid artery

(D) Blood pressure in the right radial artery

FIGURE 10 Pressure–area curves and pressure waveforms for two exemplary arteries: the right radial artery and the right common carotid artery. Normotensive state (N) is compared to the hypertensive one (H), with two different values for the parameters m and n in the tube law Equation (2). $m = 1/2$, $n = 0$ refer to the classical tube law usually adopted in previous works,[18–20] while $m = 10$, $n = -3/2$ are chosen based on experimental evidences.[34]

eutrophic remodeling,[56] that is a greater media thickness, a reduced lumen and external diameter with increased media-to-lumen ratio, without any significant change of the total amount of wall tissue. Eutrophic remodeling is accompanied by structural elevation of resistance; the main sites for vasoconstriction are the proximal resistance arteries, while the most distal resistance artery sites are partly protected from pressure elevation by a raised resistance upstream. The computed capillary pressure increases less from normotensive to hypertensive case; its pulse rises is in good agreement with the literature range.[62] The term rarefaction indicates the reduction in the number of interconnected small arteries and capillaries[59,101]; increased number of non perfused microvessels can progress in anatomic absence of microvessels.[56] Capillary rarefaction could represent an early structural abnormality in borderline hypertension and in offspring from hypertensive parents. Antonios et al.[101] studied capillaries of the skin of the dorsum of the fingers by intravital capillary microscopy in people with borderline hypertension and proved that rarefaction may precede high blood pressure and it could be an early abnormality in the progression of hypertension.

4.2.5 | Pulsatility and resistive indexes

A close relationship was established between microvascular damage in brain and kidney and indices of age and hypertension.[102] Exposure of small vessels to highly pulsatile pressure and flow explains microvascular damage and resulting

renal insufficiency and intellectual deterioration. Pulsatility index (PI) is defined as the difference between the peak systolic and minimum diastolic flow rate, divided by the mean flow rate over a cardiac cycle, or equivalently, as the difference between the peak systolic and minimum diastolic flow velocity, divided by the mean velocity over a cardiac cycle. It can be measured with non-invasive methods and it is widely used for the assessment of vascular resistance as well as for the determination of end-organ damage. Chuang et al.[103] observed a strong association between the PI in the common carotid artery and the possibility of future stroke. Cho et al.[104] measured flow velocities and PI of the middle cerebral and internal carotid arteries in 94 hypertensive patients; they observed decreased flow velocity with increased flow pulsatility in patients with a longer duration of hypertension, while no significant differences were found in patients with <5 years of hypertension. PI was also studied in the renal circulation; Petersen et al.[83] observed an association between renal artery PI and renal function parameters, such as creatinine clearance, in patients with renal failure and hypertension.

Regarding the kidney's circulation, Petersen et al.[83] measured PI and resistive index (RI) from blood flow velocities of renal arteries in normotensive and hypertensive patients; RI was calculated as the difference of peak systolic velocity and peak diastolic velocity over peak systolic velocity. They reported an increase in PI from 1.19 (0.93–1.25) to 1.65 (1.31–1.86) in hypertensive patients compared to normotensive controls; the RI increased from 0.67 (0.64–0.70) to 0.76 (0.69–0.81). Okura[105] measured PI and RI from blood flow velocity in interlobar arteries; they found PI equal to 1.30 $\pm$ 0.29 and RI equal to 0.65 $\pm$ 0.08 in a cohort of patients with essential hypertension. Our computed indexes are in line with values reported in the literature; however, computational results do not reproduce the significant rise in PI of renal arteries observed in clinical measurements. This is probably due to the fact that we do not differentiate the hypertension remodeling of the renal circulation from other vascular territories. Nevertheless, the kidneys play an inextricable role in hypertension; abnormalities in kidneys' function and sequential changes in renal haemodynamics were observed in hypertensive patients.[106] Moreover, the kidney, as the brain, is characterized by a pronounced blood flow regulation based on two mechanisms, the myogenic response and the tubulo-glomerular feedback.[107] These kidney-specific changes in renal circulation were not included in our model and could be the cause for observed discrepancies between our computational results and clinical observations.

Concerning the cerebral circulation, previous works mainly focused on carotid and middle cerebral arteries to study the haemodynamic changes associated with hypertension. Ferrara et al.[84] used ultrasound images for the evaluation of PI and a RI in the proximal segment of the internal carotid arteries and the middle cerebral arteries. Comparing normotensive and hypertensive patients, they found a PI equal to 0.84 $\pm$ 0.11 and 0.88 $\pm$ 0.19 and RI equal to 0.79 $\pm$ 0.12 and 0.81 $\pm$ 0.12, respectively, in internal carotid arteries; in middle cerebral arteries, they measured PI to be 0.54 $\pm$ 0.05 and 0.55 $\pm$ 0.07 and RI equal to 0.52 $\pm$ 0.05 and 0.52 $\pm$ 0.05 in normotensive and hypertensive patients, respectively. No significant differences were found between the healthy and the pathological groups of patients. From our computational model, we can observe that in these arteries PI tends to decrease from normotensive condition to hypertension, even if their values are comparable to literature measurements.

4.3 | The heart

4.3.1 | Left ventricle hypertrophy and its effect on elastance

Chronically increased left ventricular workload due to arterial stiffness in hypertensive patients can result in left ventricular hypertrophy, impaired relaxation, left atrial enlargement, an increased risk of arrhythmias, especially atrial fibrillation, and an increased risk of heart failure with preserved ejection fraction and heart failure with reduced ejection fraction. Structural changes of left ventricle in hypertension can be classified as concentric hypertrophy (increase in left ventricular mass and relative wall thickness), concentric remodeling (normal left ventricular mass, abnormal relative wall thickness), or eccentric hypertrophy (increased mass with normal relative wall thickness).[60,86] Remodeling usually characterizes normal aging without hypertension and it is probably an adaptation to preserve ejection fraction.[60] In case of concentric hypertrophy, the cardiac muscle cells increase in thickness by building more contractile proteins in parallel. According to the Laplace's law (5), the thicker wall with normal lumen normalizes peak systolic wall stress despite higher blood pressure. Cardiac hypertrophy acts to maintain a normal stroke volume and cardiac output through increased intraventricular pressure.

Borlaug et al.,[108] in a large cohort of hypertensive patients, concluded that arterial stiffening is matched with left ventricle systolic stiffening, with a concordant increase in E_a and E_{es}; moreover, they observed that left ventricle

hypertrophy is associated with enhanced myocardial contractility. Antihypertensive therapies could improve the ventricular-arterial coupling, by reducing both E_a and E_{es}, as pointed out by Lam et al.[109]

4.3.2 | The right heart and the pulmonary circulation

The right heart and the pulmonary circulation are not immune to the effects of systemic hypertension. Computational results in Table 5 show that the right-heart pressures among the hypertensive patients increase significantly with respect to the values in the normotensive controls. In the same way, pulmonary arterial pressure increases in hypertensive patients with respect to values observed in the normotensive scenario. Olivari et al.[66] presented the first comprehensive study on the pulmonary circulation and right ventricular function in uncomplicated hypertensive patients, comparing 16 hypertensives with left ventricle hypertrophy and 17 without it. They showed that pulmonary vascular resistance is increased compared to controls; this is unrelated to left ventricle filling pressures and it could be due to the fact that pulmonary vessels experience similar structural changes as those observed in systemic vessels. The same conclusion has been reported by Guazzi et al.[110] Moreover, Olivari et al.[66] showed decreased stroke volume as a function of right atrial pressure in patients without left ventricle hypertrophy while a preserved relation between stroke volume and right atrial pressure in patients with hypertrophy. Established cardiac hypertrophy could lead to a reduction in stroke volume in the absence of effective compensation; such compensation can be found in the form of increased cardiac filling pressure. In a previous mathematical model of arterial hypertension, Liang et al.[16] reproduced ventricular hypertrophy increasing the elastance of left ventricle without considering modifications of the pulmonary or venous systems. This leads to decreased cardiac index and stroke volume, as observed in Ganau et al.[86] in case of concentric remodeling of left ventricle in hypertensive patients. However, observing patients with concentric hypertrophy, Ganau et al.[86] found slightly increased stroke volume and cardiac index. As shown in Reference 12 by means of a simple mathematical model of the heart-arterial coupling, in case of concentric hypertrophy, the increased venous filling pressure normalizes the end-diastolic wall stress, still while normalizing the systolic wall stress; as a consequence, stroke volume and cardiac output are preserved in hypertension. Computed central venous pressure, evaluated as mean right atrial pressure, increases from 4.16 mm Hg in normotensive subject to 5.15 mm Hg in hypertension, in line with the increase observed by Safar et al.[74] (from 4.4 ± 0.6 mm Hg in normotensive controls to 5.0 ± 0.6 mm Hg in hypertensive patients). As a result, we observe an increment in maximum right atrium volume from 108.06 to 126.62 mL. While we did not consider any adaptation of the right atrium to the hypertensive condition, the increase in its volume for the hypertensive scenario with respect to the baseline volume is qualitatively in agreement with reported increased right atrium volume in hypertensive patients with respect to what observed in normotensive controls.[111] It is worth noting that authors in Reference 111 point out that a thorough characterization of changes in right atrium for arterial hypertension is currently missing. Changes in venous filling pressure could be caused by reduced venous compliance in order to produce an adequate driving pressure for the hypertrophied heart. This theory was supported by Safar and London.[73] In a more recent review on right heart and pulmonary circulation in hypertension,[112] the authors concluded that right ventricle function may be altered at an early stage of hypertension when left ventricle hypertrophy is still not evident. However, as the left ventricle remodeling progresses and pulmonary arterial pressure increases, the right ventricle becomes hypertrophic in a similar way as for the left ventricle. Figure 5 shows the computed pressure-volume loop of the right ventricle, which differs from the one obtained for the left ventricle. In particular, peak pressure is reached at a more central point[113] and the initial emptying phase shows a different behavior with respect to the one observed in the left ventricle, in agreement with clinically obtained pressure-volume curves for this chamber.[114] Moreover, the loop obtained for the hypertensive case displays a shift on the right with respect to what observed in the normotensive case. Even if the parameters that characterize the model of the right ventricle are not modified in the hypertensive scenario, our computational results display a hypertrophic behavior as a consequence of left ventricle hypertrophy and increased pulmonary arterial resistance.

4.4 | Total blood volume and vascular compliance

As discussed in the previous section, cardiac hypertrophy leads to a reduction in stroke volume in the absence of normalization of diastolic wall stress. This normalization is due to increased venous filling pressure, that could be the result of decreased venous compliance.

The vascular compliance of the circulatory system is defined as the slope of the relationship between intravascular volume and circulatory filling pressure; this property reflects the inherent elasticity of the vascular system. In animals, total vascular compliance can be obtained by determining mean circulatory filling pressure-blood volume curves. Mean circulatory filling pressure can be estimated by stopping the heart and waiting for blood to redistribute in the vascular system according to the capacity of the different districts. To avoid this methodological limitation, a different index of capacitance was introduced as a measure of total vascular compliance. This method was first presented in Reference [75]; it involves simultaneous recording of right atrial pressure and volume changes induced by transfusion, bleeding, or rapid iso-oncotic dextran infusion. London et al.[69] determined the total effective vascular compliance (TEVC) using an infusion of 500 mL of 6% dextran carried out within 4 min in a large forearm vein in control and hypertensive patients in supine position. The slope of the relationship between central venous pressure (CVP) and blood volume was called TEVC in order to differentiate it from the compliance obtained from mean circulatory filling pressure measurements. Several studies have shown that effective total vascular compliance in normal man has the character of a biological constant with values ranging from 2.1 to 2.7 mL/mm Hg/kg.[68,69,75] Total effective vascular compliance is the sum of compliances of the arterial system, which is very low in man (1%–3% of the total compliance), and the venous system, which accounts for 97%–98% of the total compliance. In patients with uncomplicated sustained essential hypertension, it was proved that total effective compliance is significantly reduced by 25% in comparison with normal subjects of the same age and sex.[69,71,74] For the same volume expansion as in normotensive controls, central venous pressure is significantly higher in hypertensive subjects. On the contrary, effective cardiopulmonary vascular compliance (evaluated as the ratio between changes in cardiopulmonary blood volume and central venous pressure during infusion) is comparable between normotensive and hypertensive patients.[67] As observed in animals,[75] these findings reflect a reduced compliance in the systemic vessels of hypertensive humans[69] and not in the cardiopulmonary circulation. The venous function can be modified by structural or functional changes, or both.[72] In animal models of hypertension,[115] venous wall hypertrophy was found in the portal vein which creates a stiffer framework on which the active contractile process is able to develop greater tension. These observations are translated into our mathematical model of arterial hypertension by reducing the venous compliance value. We observe that this modeling assumption affects only the compliance of small veins and venules, without modifying the structural properties of larger caliber veins. However, the major part of total venous compliance is distributed in the venules compartments and hence modifications of 1D veins compliance will have slight effects on total vascular compliance. Moreover, in this mathematical framework, venous compliance is reduced in hypertensive scenario without considering venous unstressed volume that is maintained equal to that of the normotensive case. Venous tone is determined by the interaction between venous compliance and unstressed volume, hence changes in unstressed volume could influence the total effective compliance determination. We chose to reduce venous compliance instead of changing unstressed volume because there is evidence of stiffening in rats' veins.[115] Total effective vascular compliance was computationally estimated in our model by means of an infusion of 500 mL of blood, as described in Reference [25].

The role of the veins in modeling hypertension had received little attention. However, since approximately two-thirds of the systemic blood is normally contained in venous circulation, this variation in vascular compliance has important consequences on the venous vasculature, as well as on the overall circulation. The decreased venous compliance produces a redistribution of blood volume; since total blood volume is normal or reduced and there is no decrease in the compliance of the cardiopulmonary circulation,[67,73,75] this results in a shift of blood to the central circulation (heart and lungs). Figure 7 shows the blood volume distribution in the main districts of the circulation: arterial blood (1D arteries, small arteries and arterioles), capillaries, venous blood (venules, small veins and 1D veins), heart and pulmonary circulation. It can be observed that in the hypertensive case, the arterial and capillaries percentages of blood volume are comparable to the normotensive state, but there is a slight increase in heart and pulmonary circulation amount of blood (+3%), matched by a small decrease in venous blood. London et al.[71] reported that the percentage of cardiopulmonary blood volume with respect to total blood volume was 23 ± 1 in normotensive group while 25 ± 1 in hypertensive group; in another study by the same leading author,[67] the cardiopulmonary blood volume was increased by about 7% in hypertensive subjects with respect to the healthy controls. The shift in central blood volume is caused by the reduced venous compliance, which decreases the capacity of the venous system to accommodate enough blood volume. As a consequence of the shift of blood to the central circulation (heart and lungs), filling pressure and cardiac output slightly increase. Ulrych et al.[116] showed that the increase in cardiac output following an intravenous volume load was exaggerated in hypertensive patients, suggesting a reduction in peripheral vascular capacity. Moreover, there is an inverse correlation between cardiac output and vascular compliance in hypertensive subjects: the greater the reduction in the compliance, the higher the cardiac output.

4.5 | The venous system

For years, it was thought that the main role of the venous circulation was returning blood to the heart; it is now recognized that systemic veins perform other important functions. As stressed in the previous section, the venous system serves as a blood reservoir for the entire circulation; it is able to store a highly variable amount of blood and to make it available when required for several reasons, such as cardiac output regulation.

Beyond the role played by the decreased venous compliance, the behavior of the venous system in essential hypertension has not been often considered in the literature. Novo et al.[117] showed that the arm venous pressure in hypertensive patients and in elderly patients with systolic hypertension is higher compared to that measured in healthy controls; the authors concluded that in essential hypertension, both the arterial and the venous circulatory systems are characterized by increased pressure. In a recent study on chronic venous insufficiency,[118] the authors supported the thesis of an interdependence of venous and arterial hypertension. Rubira et al.[119] showed that endothelial dysfunction that usually characterized arteries was also present in the venous system of hypertensive patients. Moreover, a recent review[120] stressed the importance of cellular and molecular mechanisms of aging processes of veins and their similarities with those of the arterial system.

From our computational results, one can observe that venous pressure increases by about 20% in all selected veins. The venous pulse pressure increases in the hypertensive scenario with respect to that obtained the normotensive state. According to the pressure-area relationship of large veins, higher venous pressure range results in higher pulse amplitude. However, this holds if we model reduced venous compliance without considering unstressed volume changes; indeed, unstressed volume modification would translate the pressure-area curve, resulting in higher venous pressure without significant changes in pulsatility. Taking in mind our modeling assumption, computational results reveal that arterial hypertension leads to venous hypertension and increased venous pulse pressure, both in systemic and cerebral venous circulation. Chung et al.[121] hypothesized that chronic elevated cerebral venous pressure might cause cerebral venule hypertension, resulting in reduced cerebral blood flow, altered microvessel structures, impair cerebral autoregulation; these consequences would lead to chronic cerebral ischaemia and leukoaraiosis pathology. Moreover, increased cerebral venous pressure may impair the cerebrospinal fluid system dynamics.[122]

Despite little evidence on the characteristics of the venous circulation in essential hypertension, our computational results show that this vascular district is also affected, displaying venous hypertension, increased flow rate and increased pulsatility of both pressure and flow waveforms. Chung et al.[121] stressed that only a compliant vein can accommodate the increased venous pressure by effective distension to maintain a normal venous pressure; decreased venous compliance was found in normotensive men with positive family histories of hypertension and in borderline hypertension. This might indicate that reduced venous compliance is present before hypertension is developed, contributing to the pathogenesis of hypertension.

4.6 | Limitations

The major limitation of this work is that haemodynamic changes on the global model due to hypertension were calibrated to population-averaged data or previous mathematical studies. However, haemodynamic conditions largely differ among patients, due to age, weight, to name but a few; patient-specific characteristics and remodeling could improve the model-based theoretical insights on specific hypertensive status. To be viable, large data support from in vivo studies would be required. A step forward could be done considering different hypertensive scenarios, at different ages and stages of the disease. Another aspect which deserves attention is the role played by other regulatory systems of arterial pressure, in particular the body fluids control in long-term regulation and its implication in the hypertension of renal origin. Future works could address the interaction between blood volume and extracellular fluids, as well as their regulation. The role played by the microcirculation in hypertension, as well as in aging, is a popular topic in the clinical literature.[62,123–127] In this paper, the microcirculation was simplified as lumped resistor-capacitor compartments. Remodeling in the microcirculation due to hypertension involves structural modifications and rarefaction processes that are simply translated into an increase in vascular resistance. However, a more realistic microvascular networks model would better capture the consequence of the remodeling. In the clinic, an open question remains about the microcirculation: is it affected in the same way in all peripheral beds? Especially for capillaries, it can be possible to measure their pressure only in the skin. Mathematical models could help in elucidating this issue. Finally, we point out that the pressure waveform obtained in the radial artery shows a pulse pressure that is smaller than what would expect for a young subject.[128] This is linked to

observed values for augmentation index and pulse pressure amplification reported in Table 2, which are smaller than the reference ones. While this is something that should be improved in future versions of the model, we observe that our results reproduce trends from normo- to hypertensive conditions in a correct manner.

5 | CONCLUSIONS

We have introduced the functional and structural changes that are cause/consequence of arterial hypertension into a global multi-scale closed-loop model of the entire circulation in order to simulate the interplay between different vascular compartments in the pathological state. To the best of our knowledge, this is the first time that this disease is studied in a global closed-loop context by means of a model which comprises both one-dimensional representation of main large to medium size arteries and other major compartments of the blood circulation, in particular the venous system, that is represented by means of one-dimensional systems of equations for major veins and zero-dimensional models for small veins and venules. In a previous mathematical work,[16] the authors focused on one-dimensional network of arteries to assess the wave propagation and the increase in wave velocity that is usually observed in hypertensive patients; even if they used a closed-loop model, they did not considered the effect of reduced venous compliance. Another completely lumped-parameter approach was adopted in global models for system analysis of arterial pressure, such as the work by Guyton.[4] The work presented in this paper permits to study both the wave propagation in the arterial system and the function of the venous circulation in developing high blood pressure and controlling cardiac output. An important aspect of this work is the introduction of total blood volume, which comprises both stressed and unstressed components, that together with vascular capacitance, play a role in the determination of arterial pressure. The short-term regulation of pressure due to baroreflex has been introduced in the global model and reset to high blood pressure levels in the hypertensive scenario. The leading role of the baroreflex in short-term regulation of arterial pressure is well established in the literature; more recent studies have posed doubts about its complex and long-term role in hypertension. Its introduction in the global model of circulation represents an added value for the study of hypertension. In fact, its role is crucial for estimating total effective vascular compliance. As pointed out in a previous work,[25] the physiological parametrization of the mathematical model, in particular the assignment of physical compliance and unstressed volume in different vascular compartments, is necessary but not sufficient for the determination of total effective vascular compliance values in agreement with experimental data[69]; major physiological mechanisms, in particular the short-term control of arterial pressure, are needed to obtain modeling results that are in agreement with observed variations in mean arterial pressure, cardiac output, heart rate, and cardiopulmonary blood volume during the infusion test.

The mathematical work presented here represents a baseline model for different applications in hypertensive context. Future works will focus on assess the major determinants of arterial hypertension by means of sensitivity analysis, as well as on specific vascular territories, like the cerebral circulation.

DATA AVAILABILITY STATEMENT
The data that support the findings of this study are available from the corresponding author upon reasonable request.

ORCID
Giulia Bertaglia https://orcid.org/0000-0002-2874-9588
Valerio Caleffi https://orcid.org/0000-0001-7066-4804
Pablo J. Blanco https://orcid.org/0000-0003-3527-619X
Lucas O. Müller https://orcid.org/0000-0003-1933-8995

REFERENCES
1. Herring N, Paterson DJ. *Levick's Introduction to Cardiovascular Physiology*. 6th ed. Routledge; 2018:449.
2. Mancia G, Rosei EA, Azizi M, et al. 2018 ESC/ESH guidelines for the management of arterial hypertension. *Eur Heart J*. 2018;39:3021-3104.

3. W. H. Organization. *A Global Brief on Hypertension*. W. H. Organization; 2013.

4. Guyton AC, Coleman TG, Cowley AW, Liard J, Norman RA, Manning RD. Systems analysis of arterial pressure regulation and hypertension. *Ann Biomed Eng*. 1972;1(2):254-281.

5. Hall JE, Guyton AC. *Guyton and Hall Textbook of Medical Physiology*. 12th ed. Saunders/Elsevier; 2011.

6. Beard DA, Pettersen KH, Carlson BE, Omholt SW, Bugenhagen SM. A computational analysis of the long-term regulation of arterial pressure. *F1000Res*. 2003;2:208.

7. Carthy ER. Autonomic dysfunction in essential hypertension: a systematic review. *Ann Med Surgry*. 2014;3(1):2-7.

8. Parmer RJ, Cervenka JH, Stone RA. Baroreflex sensitivity and heredity in essential hypertension. *Circulation*. 1992;85(2):497-503.

9. Abram SR, Hodnett BL, Summers RL, Coleman TG, Hester RL. Quantitative circulatory physiology: an integrative mathematical model of human physiology for medical education. *Teach Technol*. 2007;31:9.

10. Karaaslan F, Denizhan Y, Hester R. A mathematical model of long-term renal sympathetic nerve activity inhibition during an increase in sodium intake. *Am J Physiol Regul Integr Comp Physiol*. 2014;306(4):R234-R247.

11. Karaaslan F, Denizhan Y, Kayserilioglu A, Gulcur HO. Long-term mathematical model involving renal sympathetic nerve activity, arterial pressure, and sodium excretion. *Ann Biomed Eng*. 2005;33(11):1607-1630.

12. Segers P, Stergiopulos N, Verdonck P, Westerhof N. Mathematical model analysis of heart-arterial interaction in hypertension. *2001 Conference Proceedings of the 23rd Annual International Conference of the IEEE Engineering in Medicine and Biology Society, Istanbul, Turkey*. Vol 1. IEEE; 2001:192-195.

13. Charlton PH, Mariscal Harana J, Vennin S, Li Y, Chowienczyk P, Alastruey J. Modeling arterial pulse waves in healthy aging: a database for in silico evaluation of hemodynamics and pulse wave indexes. *Am J Physiol Heart Circ Phys Ther*. 2019;317(5):H1062-H1085.

14. Li Y, Gu H, Fok H, Alastruey J, Chowienczyk P. Forward and backward pressure waveform morphology in hypertension. *Hypertension*. 2017;69(2):375-381.

15. Blanco PJ, Müller LO, Spence JD. Blood pressure gradients in cerebral arteries: a clue to pathogenesis of cerebral small vessel disease. *Stroke Vasc Neurol*. 2017;2(3):108-117.

16. Liang F, Guan D, Alastruey J. Determinant factors for arterial hemodynamics in hypertension: theoretical insights from a computational model-based study. *J Biomech Eng*. 2018;140(3):031006.

17. Canuto D, Chong K, Bowles C, Dutson EP, Eldredge JD, Benharash P. A regulated multiscale closed-loop cardiovascular model, with applications to hemorrhage and hypertension. *Int J Numer Method Biomed Eng*. 2018;34(6):e2975.

18. Müller LO, Toro EF. Enhanced global mathematical model for studying cerebral venous blood flow. *J Biomech*. 2014;47(13):3361-3372.

19. Müller LO, Toro EF. A global multiscale mathematical model for the human circulation with emphasis on the venous system. *Int J Numer Methods Biomed Eng*. 2014;30(7):681-725.

20. Toro EF, Celant M, Zhang Q, et al. Cerebrospinal fluid dynamics coupled to the global circulation in holistic setting: mathematical models, numerical methods and applications. *Int J Numer Methods Biomed Eng*. 2021;38:e3532.

21. Ursino M, Lodi CA. A simple mathematical model of the interaction between intracranial pressure and cerebral hemodynamics. *J Appl Physiol*. 1997;82(4):1256-1269.

22. Payne S. A model of the interaction between autoregulation and neural activation in the brain. *Math Biosci*. 2006;204:260-281.

23. Ursino M, Giannessi M. A model of cerebrovascular reactivity including the circle of Willis and cortical anastomoses. *Ann Biomed Eng*. 2010;38:955-974.

24. Blanco P, Trenhago P, Fernandes L, Feijóo R. On the integration of the baroreflex control mechanism in a heterogeneous model of the cardiovascular system: modeling the baroreflex mechanism in the cardiovascular system. *Int J Numer Methods Biomed Eng*. 2012;28(4):412-433.

25. Celant M, Toro EF, Müller LO. Total effective vascular compliance of a global mathematical model for the cardiovascular system. *Symmetry*. 2021;13(10):1858.

26. Sun Y, Beshara M, Lucariello R, Chiaramida S. A comprehensive model for right–left heart interaction under the influence of pericardium and baroreflex. *Am J Physiol*. 1997;272:H1499-H1515.

27. Mynard J, Davidson M, Penny D, Smolich J. A simple, versatile valve model for use in lumped parameter and one-dimensional cardiovascular models. *Int J Numer Methods Biomed Eng*. 2012;28:626-641.

28. Ursino M. A mathematical study of human intracranial hydrodynamics part 1 – the cerebrospinal fluid pulse pressure. *Ann Biomed Eng*. 1988;16(4):379-401.

29. Payne S. *Cerebral Autoregulation. Control of Blood Flow in the Brain*. 1st ed. Springer; 2016.

30. Toro EF, Santacá A, Montecinos GI, Celant M, Müller LO. AENO: a novel reconstruction method in conjunction with ADER schemes for hyperbolic equations. *Commun Appl Math Comput*. 2023;5:776-852.

31. Danielsen M. *Modeling of Feedback Mechanisms which Control the Heart Function in a View to an Implementation in Cardiovascular Models*. PhD thesis. Roskilde University Center; 1998.

32. Toro EF. The ADER path to high-order Godunov methods. *Continuum Mechanics, Applied Mathematics and Scientific Computing: Godunov's Legacy – ALiber Amicorum to Professor Godunov*. Springer Verlag; 2020:359-366.

33. Toro EF, Siviglia A. Flow in collapsible tubes with discontinuous mechanical properties: mathematical model and exact solutions. *Commun Comput Phys*. 2013;13(2):361-385.

34. Colombo C. *Mathematical Properties-Preserving Parameter Estimation for a Blood Flow Model Using Ovine and Human in Vitro Data*. Master's thesis. University of Trento, Department of Mathematics; 2020.

35. Olufsen M. Structured tree outflow condition for blood flow in larger systemic arteries. *Am J Physiol Heart Circ Physiol*. 1999;276:H257-H268.

36. Nippa JH, Alexander RH, Folse R. Pulse wave velocity in human veins. *J Appl Physiol*. 1971;30:558-563.

37. Liang F, Takagi S, Himeno R, Liu H. Biomechanical characterization of ventricular–arterial coupling during aging: a multi-scale model study. *J Biomech*. 2009;42(6):692-704.

38. Mynard J, Smolich J. One-dimensional haemodynamic modeling and wave dynamics in the entire adult circulation. *Ann Biomed Eng*. 2015;43:1443-1460.

39. Alastruey J, Khir AW, Matthys KS, et al. Pulse wave propagation in a model human arterial network: assessment of 1-D visco-elastic simulations against in vitro measurements. *J Biomech*. 2011;44(12):2250-2258.

40. Cattaneo C. A form of heat-conduction equations which eliminates the paradox of instantaneous propagation. *C R Math l'Acad Sci*. 1958;247:431-433.

41. Toro E, Millington R, Nejad L. Towards very high–order Godunov schemes. In: Toro E, ed. *Godunov Methods: Theory and Applications. Edited Review*. Kluwer Academic/Plenum Publishers; 2001:905-937.

42. Montecinos G, Müller L, Toro E. Hyperbolic reformulation of a 1D viscoelastic blood flow model and ADER finite volume schemes. *J Comput Phys*. 2014;266:101-123.

43. Montecinos GI, Toro EF. Reformulations for general advection-diffusion-reaction equations and locally implicit ADER schemes. *J Comput Phys*. 2014;275:415-442.

44. Müller L, Parés C, Toro E. Well-balanced high-order numerical schemes for one-dimensional blood flow in vessels with varying mechanical properties. *J Comput Phys*. 2013;242:53-85.

45. Müller L, Toro E. Well-balanced high-order solver for blood flow in networks of vessels with variable properties. *Int J Numer Methods Biomed Eng*. 2013;29:1388-1411.

46. Toro E, Montecinos G. Advection-diffusion-reaction equations: hyperbolisation and high-order ADER discretizations. *SIAM J Sci Comp*. 2014;36:A2423-A2457.

47. Dumbser M, Käser M, Toro EF. An arbitrary high order discontinuous galerkin method for elastic waves on unstructured meshes v: local time stepping and p–adaptivity. *Geophys J Int*. 2007;171:695-717.

48. Müller LO, Blanco PJ, Watanabe SM, Feijóo RA. A high-order local time stepping finite volume solver for one-dimensional blood flow simulations: application to the ADAN model. *Int J Numer Methods Biomed Eng*. 2016;32(10).

49. Müller L, Blanco P. A high order approximation of hyperbolic conservation laws in networks: application to one-dimensional blood flow. *J Comput Phys*. 2015;300:423-437.

50. Müller L, Leugering G, Blanco P. Consistent treatment of viscoelastic effects at junctions in one-dimensional blood flow models. *J Comput Phys*. 2016;314:167-193.

51. Ursino M, Innocenti M. Modeling arterial hypotension during hemodialysis. *Artif Organs*. 2008;21(8):873-890.

52. McEniery CM, Wilkinson IB, Avolio AP. Age, hypertension and arterial function. *Clin Exp Pharmacol Physiol*. 2007;34(7):665-671.

53. McEniery CM, Yasmin, Hall IR, Qasem A, Wilkinson IB, Cockcroft JR. Normal vascular aging: differential effects on wave reflection and aortic pulse wave velocity. *J Am Coll Cardiol*. 2005;46(9):1753-1760.

54. Bussy C, Boutouyrie P, Lacolley P, Challande P, Laurent S. Intrinsic stiffness of the carotid arterial wall material in essential hypertensives. *Hypertension*. 2000;35(5):1049-1054.

55. Feihl F, Liaudet L, Waeber B. The macrocirculation and microcirculation of hypertension. *Curr Hypertens Rep*. 2009;11(3):182-189.

56. Laurent S, Boutouyrie P. The structural factor of hypertension: large and small artery alterations. *Circ Res*. 2015;116(6):1007-1021.

57. Laurent S, Girerd X, Mourad JJ, et al. Elastic modulus of the radial artery wall material is not increased in patients with essential hypertension. *Arterioscler Thromb: J Vasc Biol*. 1994;14(7):1223-1231.

58. Farasat SM, Morrell CH, Scuteri A, et al. Do hypertensive individuals have enlarged aortic root diameters? Insights from studying the various subtypes of hypertension. *Am J Hypertens*. 2008;21(5):558-563.

59. Levy B, Ambrosio G, Pries A, Struijker-Boudier H. Microcirculation in hypertension: a new target for treatment? *Circulation*. 2001;104(6):735-740.

60. Mayet J. Cardiac and vascular pathophysiology in hypertension. *Heart*. 2003;89(9):1104-1109.

61. Rizzoni D, Agabiti-Rosei E. Structural abnormalities of small resistance arteries in essential hypertension. *Intern Emerg Med*. 2012;7(3):205-212.

62. James MA, Tullett J, Hemsley AG, Shore AC. Effects of aging and hypertension on the microcirculation. *Hypertension*. 2006;47(5):968-974.

63. McEniery CM, Yasmin, McDonnell B, et al. Central pressure: variability and impact of cardiovascular risk factors: the Anglo-Cardiff collaborative trial II. *Hypertension*. 2008;51(6):1476-1482.

64. Abdelhammed A, Smith R, Levy P, Smits G, Ferrario C. Noninvasive hemodynamic profiles in hypertensive subjects. *Am J Hypertens*. 2005;18(2):51-59.

65. Lund-Johansen P. Haemodynamics in essential hypertension. *Clin Sci*. 1980;59(s6):343s-354s.

66. Olivari MT, Fiorentini C, Polese A, Guazzi MD. Pulmonary hemodynamics and right ventricular function in hypertension. *Circulation*. 1978;57(6):1185-1190.

67. London GM, Safar ME, Payen DM, Gitelman RC, Guerin AM. Total, peripheral and intrathoracic effective compliances of the vascular bed in normotensive and hypertensive patients. In: Bahlmann J, Liebau H, eds. *Contributions to Nephrology*. Vol 30. S. Karger AG; 1982:144-153.

68. Safar ME, London GM, Simon AC, Weiss YA, eds. *Arterial and Venous Systems in Essential Hypertension, Volume 63 of Developments in Cardiovascular Medicine*. Springer; 1987.

69. London G, Safar M, Weiss Y, Simon C. Total effective compliance of the vascular bed in essential hypertension. *Am Heart J*. 1978;95(3): 325-330.

70. London GM, Guerin AP, Marchais SJ, Pannier B, Safar M, Day M. Cardiac and arterial interactions in end-stage renal disease. *Kidney Int*. 1996;50(2):600-608.

71. London GM, Safar ME, Simon AC, Alexandre JM, Levenson JA, Weiss YA. Total effective compliance, cardiac output and fluid volumes in essential hypertension. *Circulation*. 1978;57(5):995-1000.

72. Safar ME, London GM. Venous system in essential hypertension. *Clin Sci*. 1985;69(5):497-504.

73. Safar ME, London GM. Arterial and venous compliance in sustained essential hypertension. *Hypertension*. 1987;10(2):133-139.

74. Safar ME, London GM, Levenson JA, Simon AC, Chau NP. Rapid dextran infusion in essential hypertension. *Hypertension*. 1979;1(6): 615-623.

75. Echt M, Duweling J, Gauer OH, Lange L. Effective compliance of the total vascular bed and the intrathoracic compartment derived from changes in central venous pressure induced by volume changes in man. *Circ Res*. 1974;34:8-68.

76. Cipolla MJ, Liebeskind DS, Chan S. The importance of comorbidities in ischemic stroke: impact of hypertension on the cerebral circulation. *J Cereb Blood Flow Metab*. 2018;38(12):2129-2149.

77. Mussalo H, Vanninen E, Ikäheimo R, et al. Baroreflex sensitivity in essential and secondary hypertension. *Clin Auton Res*. 2002;12(6): 465-471.

78. Li J, Peng Y, Ji K. Brachial pulse pressure is associated with the presence and extent of coronary artery disease in stable angina patients: a cross-sectional study. *BMC Cardiovasc Disord*. 2020;20(1):143.

79. Asmar RG, Benetos A, London GM, et al. Aortic distensibility in normotensive, untreated and treated hypertensive patients. *Blood Press*. 1995;4(1):48-54.

80. Tanaka H, Munakata M, Kawano Y, et al. Comparison between carotid-femoral and brachial-ankle pulse wave velocity as measures of arterial stiffness. *J Hypertens*. 2009;27(10):2022-2027.

81. Kaibe M, Ohishi M, Komai N, et al. Arterial stiffness index: a new evaluation for arterial stiffness in elderly patients with essential hypertension: ASI in elderly hypertensive patients. *Geriatr Gerontol Int*. 2002;2(4):199-205.

82. Laurent S, Caviezel B, Beck L, et al. Carotid artery distensibility and distending pressure in hypertensive humans. *Hypertension*. 1994; 23(6_pt_2):878-883.

83. Petersen LJ, Petersen J, Ladefoged S, Mehlsen J, Jensen H. The pulsatility index and the resistive index in renal arteries in patients with hypertension and chronic renal failure. *Nephrol Dial Trans*. 1995;10:2060-2064.

84. Ferrara LA, Mancini M, Iannuzzi R, et al. Carotid diameter and blood flow velocities in cerebral circulation in hypertensive patients. *Stroke*. 1995;26(3):418-421.

85. Ferlinz J. Right ventricular performance in essential hypertension. *Circulation*. 1980;61(1):156-162.

86. Ganau A, Devereux RB, Roman MJ, et al. Patterns of left ventricular hypertrophy and geometric remodeling in essential hypertension. *J Am Coll Cardiol*. 1992;19(7):1550-1558.

87. Bonnet B, Jourdan F, du Cailar G, Fesler P. Noninvasive evaluation of left ventricular elastance according to pressure-volume curves modeling in arterial hypertension. *Am J Physiol – Heart Circ Physiol*. 2017;313(2):H237-H243.

88. Murgo JP, Westerhof N, Giolma J, Altobelli S. Aortic input impedance in normal man: relationship to pressure wave forms. *Circulation*. 1980;62:105-116.

89. Wolf R, King B, Torres V, Wilson D, Ehman R. Measurement of normal renal artery blood flow: cine phase-contrast MR imaging vs clearance of p-aminohippurate. *Am J Roentgenol*. 1993;161:995-1002.

90. Zitnik R, Rodich F, Marshall H, Wood E. Continuously recorded changes of thoracic aortic blood flow in man in response to leg exercise in supine position. *Circ Res*. 1965;17:97-105.

91. Cheng C, Herfkens R, Taylor C. Inferior vena caval hemodynamics quantified in vivo at rest and during cycling exercise using magnetic resonance imaging. *Am J Physiol Heart Circ Physiol*. 2002;284:H1161-H1167.

92. Benetos A, Laurent S, Asmar R, Lacolley P. Large artery stiffness in hypertension. *J Hypertens*. 1997;15(2):S89-S97.

93. Nichols WW, MacDonald DA. *McDonald's Blood Flow in Arteries: Theoretical, Experimental and Clinical Principles*. 6th ed. Hodder Arnold; 2011.

94. Safar ME, Bouthier JA, Levenson JA, Simon AC. Peripheral large arteries and the response to antihypertensive treatment. *Hypertension*. 1983;5(5):III63-III68.

95. Simon AC, Laurent S, Levenson JA, Bouthier JE, Safar ME. Estimation of forearm arterial compliance in normal and hypertensive men from simultaneous pressure and flow measurements in the brachial artery, using a pulsed Doppler device and a first-order arterial model during diastole. *Cardiovasc Res*. 1983;17(6):331-338.

96. Safar ME, Blacher J, Mourad JJ, London GM. Stiffness of carotid artery wall material and blood pressure in humans: application to antihypertensive therapy and stroke prevention. *Stroke*. 2000;31(3):782-790.

97. Munakata M. Brachial-ankle pulse wave velocity in the measurement of arterial stiffness: recent evidence and clinical applications. *Curr Hypertens Rev*. 2014;10(1):49-57.

98. Shimizu M, Kario K. Review: role of the augmentation index in hypertension. *Ther Adv Cardiovasc Dis*. 2008;2(1):25-35.

99. Alfie J, Waisman GD, Galarza CR, Cámera MI. Contribution of stroke volume to the change in pulse pressure pattern with age. *Hypertension*. 1999;34(4):808-812.

100. Mynard JP. *Computer modelling and wave intensity analysis of perinatal cardiovascular function and dysfunction*. PhD thesis. Department of Paediatrics, The University of Melbourne, Heart Research Group, Murdoch Childrens Research Institute; 2011.

101. Antonios TFT. Rarefaction of skin capillaries in normotensive offspring of individuals with essential hypertension. *Heart*. 2003;89(2):175-178.

102. O'Rourke MF, Safar ME. Relationship between aortic stiffening and microvascular disease in brain and kidney: cause and logic of therapy. *Hypertension*. 2005;46(1):200-204.

103. Chuang S, Cheng H, Bai C, Yeh W, Chen J, Pan W. Blood pressure, carotid flow pulsatility, and the risk of stroke: a community-based study. *Stroke*. 2016;47(9):2262-2268.

104. Cho SJ, Sohn YH, Kim GW, Kim J. Blood flow velocity changes in the middle cerebral artery as an index of the chronicity of hypertension. *J Neurol Sci*. 1997;150(1):77-80.

105. Okura T. Intrarenal and carotid hemodynamics in patients with essential hypertension. *Am J Hypertens*. 2004;17(3):240-244.

106. Coffman TM. The inextricable role of the kidney in hypertension. *J Clin Investig*. 2014;124(6):2341-2347.

107. Just A. Mechanisms of renal blood flow autoregulation: dynamics and contributions. *Am J Physiol Regul Integr Comp Physiol*. 2007; 292(1):R1-R17.

108. Borlaug BA, Lam CS, Roger VL, Rodeheffer RJ, Redfield MM. Contractility and ventricular systolic stiffening in hypertensive heart disease. *J Am Coll Cardiol*. 2009;54(5):410-418.

109. Lam CSP, Shah AM, Borlaug BA, et al. Effect of antihypertensive therapy on ventricular-arterial mechanics, coupling, and efficiency. *Eur Heart J*. 2013;34(9):676-683.

110. Guazzi MD, Polese A, Bartorelli A, Loaldi A, Fiorentini C. Evidence of a shared mechanism of vasoconstriction in pulmonary and systemic circulation in hypertension: a possible role of intracellular calcium. *Circulation*. 1982;66(4):881-886.

111. Cicco S, Calvanese C, Susca N, et al. Right atrium enlargement is related to increased heart damage and mortality in well-controlled hypertension. *Nutr Metab Cardiovasc Dis*. 2022;32(2):420-428.

112. Vriz O, Motoji Y, Ferrara F, Bossone E, Naeije R. The right heart-pulmonary circulation unit in systemic hypertension. *Heart Fail Clin*. 2018;14(3):247-253.

113. Redington AN, Gray HH, Hodson ME, Rigby ML, Oldershaw PJ. Characterisation of the normal right ventricular pressure-volume relation by biplane angiography and simultaneous micromanometer pressure measurements. *Br Heart J*. 1988;59(1):23-30.

114. Vonk-Noordegraaf A, Westerhof N. Describing right ventricular function. *Eur Respir J*. 2013;41(6):1419-1423.

115. Greenberg S, Bohr D. Venous smooth muscle in hypertension: enhanced contractility of portal veins from spontaneously hypertensive rats. *Circ Res*. 1975;36:208-215.

116. Ulrych M, Frohlich ED, Tarazi RC, Dustan HP, Page IH. Cardiac output and distribution of blood volume in central and peripheral circulations in hypertensive and normotensive man. *Heart*. 1969;31(5):570-574.

117. Novo S, Pernice C, Abrignani M, Tantillo R, Mansueto S, Strano A. Behaviour of arm venous pressure in patients with systodiastolic hypertension and in the elderly with isolated systolic hypertension in comparison with healthy controls. *Int Angiol: J Int Union Angiol*. 1997;16(2):129-133.

118. Prochaska JH, Arnold N, Falcke A, et al. Chronic venous insufficiency, cardiovascular disease, and mortality: a population study. *Eur Heart J*. 2021;42(40):4157-4165.

119. Rubira MC, Consolim-Colombo FM, Rabelo ER, et al. Venous or arterial endothelium evaluation for early cardiovascular dysfunction in hypertensive patients? *J Clin Hypertens*. 2007;9(11):859-865.

120. Molnár AÁ, Nádasy GL, Dörnyei G, et al. The aging venous system: from varicosities to vascular cognitive impairment. *GeroScience*. 2021;43(6):2761-2784.

121. Chung CP, Hsu HY, Chao AC, Cheng CY, Lin SJ, Hu HH. Jugular venous reflux affects ocular venous system in transient monocular blindness. *Cerebrovasc Dis*. 2010;29(2):122-129.

122. Beggs CB. Venous hemodynamics in neurological disorders: an analytical review with hydrodynamic analysis. *BMC Med*. 2013;11:142.

123. Li L, Mac-Mary S, Marsaut D, et al. Age-related changes in skin topography and microcirculation. *Arch Dermatol Res*. 2006;297(9): 412-416.

124. Mulvany M. Vascular remodelling of resistance vessels: can we define this? *Cardiovasc Res*. 1999;41(1):9-13.

125. Park JB, Schiffrin EL. Small artery remodeling is the most prevalent (earliest?) form of target organ damage in mild essential hypertension. *J Hypertens*. 2001;19(5):921-930.

126. Poole DC, Behnke BJ, Musch TI. Capillary hemodynamics and oxygen pressures in the aging microcirculation. *Microcirculation*. 2006; 13(4):289-299.

127. Schiffrin E. Remodeling of resistance arteries in essential hypertension and effects of antihypertensive treatment. *Am J Hypertens*. 2004; 17(12):1192-1200.

128. Reymond P, Merenda F, Perren F, Rüfenacht D, Stergiopulos N. Validation of a one-dimensional model of the systemic arterial tree. *Am J Physiol Heart Circ Physiol*. 2009;297(1):H208-H222.

APPENDIX A

This appendix summarizes the main modeling equations for 1D blood vessels (arteries and veins), for main 0D compartments and for the regulatory mechanisms adopted in this work. For each set of equations, the list of parameters and the main references are reported. These include works from other research groups on which the equations are based but mainly previous works from the authors, where the reader can find more details about the model and its parametrization. In particular, we refer to Reference 20 for a detailed description of the model, a summary of the numerical method and the complete list of the parameters.

TABLE A1 Main modeling equations of the global model for the entire circulation.

Model equations		References
1D vessels		
(A1) $\partial_t A + \partial_x q = 0$	A, q, p: cross-sectional area, flow, pressure	19
$\partial_t q + \partial_x \left(\frac{q^2}{A} \right) + \frac{A}{\rho} \partial_x p = -f$	$\hat{\alpha}$: Coriolis coefficient	18
	ρ: blood density	20
	f: friction force	
(A2) $p - p_{ext} = K\Phi(A, A_0) + P_0 + \frac{\Gamma}{A_0 \sqrt{A}} \partial_t A$	p_{ext}: external pressure	
	K: vessel wall stiffness	
	P_0: reference pressure	
	A_0: reference area	
	Γ: viscoelastic parameter	
(A3) $\Phi(A; A_0) = \left(\left(\frac{A}{A_0} \right)^m - \left(\frac{A}{A_0} \right)^n \right)$	m, n: real numbers	
(A4) $\Gamma = \frac{2}{3}\sqrt{\pi}\gamma h_0$	γ: wall viscosity	
	h_0: wall thickness	
(A5) $f = \frac{8\mu\pi}{\rho} \frac{q}{A}$	μ: blood dynamic viscosity	
Microcirculation		
(A6) $\frac{dP}{dt} = \frac{1}{C}(Q_{in} - Q) + \frac{dP_{ext}}{dt}$	P, Q: pressure, flow of arterioles (al), capillaries (cp), venules (vn)	19
$Q = \frac{P - P_{out}}{R}$	C: compliance (C_{al}, C_{cp}, C_{vn})	20
	R: resistance (R_{al}, R_{cp}, R_{vn})	
	Q_{in}: entering flow from neighbor 0D or 1D element	
	P_{out}: pressure to neighbor 0D or 1D element	
	P_{ext}: external pressure	
Heart		
(A7) $P_{ch} = P_{peri} + E(t)(V_{ch} - V_{ch,0}) + \gamma P_{ch} \frac{dV_{ch}}{dt}$	P_{ch}: chamber pressure	26
	P_{peri}: pericardial pressure	19
	$E(t)$: time-varying elastance	20
	V_{ch}: cardiac volume	
	$V_{ch,0}$: unstressed volume	
	$\gamma P_{ch}(t)$: viscoelasticity coefficient	
(A8) $P_{peri} = \exp\left(\frac{V_H - V_{PC}}{\Phi_{PC}} \right)$	$V_H(t)$: sum of the volume of the heart chambers	
	V_{PC}, Φ_{PC}: constant pericardial parameters	
(A9) $E(t) = E_A e(t) + E_B$	E_A, E_B: active and passive elastances	

TABLE A1 (Continued)

Model equations	References
(A10) $e_a(t) = \begin{cases} \frac{1}{2}\{1 + \cos[\pi(t + T - t_{ar})/T_{arp}]\} & 0 \le t \le t_{ar} + T_{arp} - T \\ 0 & t_{ar} + T_{arp} - T < t \le t_{ac} \\ \frac{1}{2}\{1 - \cos[\pi(t - t_{ac})/T_{acp}]\} & t_{ac} < t \le t_{ac} + T_{acp} \\ \frac{1}{2}\{1 + \cos[\pi(t - t_{ar})/T_{arp}]\} & t_{ac} + T_{acp} < t \le T \end{cases}$	
$e_a(t)$: normalized time-varying elastance for atria	
T: cardiac cycle duration	
t_{ar}, t_{ac}: atrial relaxation/contraction begin	
T_{arp}, T_{acp}: atrial relaxation/contraction duration	
(A11) $e_v(t) = \begin{cases} \frac{1}{2}[1 - \cos(\pi t/T_{vcp})] & 0 \le t \le T_{vcp} \\ \frac{1}{2}\{1 + \cos[\pi(t - T_{vcp})/T_{vrp}]\} & T_{vcp} < t \le T_{vcp} + T_{vrp} \\ 0 & T_{vcp} + T_{vrp} < t \le T \end{cases}$	
$e_v(t)$: normalized time-varying elastance for ventricles	
T_{vrp}, T_{vcp}: ventricular relaxation/contraction duration	

Pulmonary circulation

(A12)	$p = E\Phi$	p is pressure in each pulmonary compartment—arteries (A), capillaries (cp), veins (V)	26
(A13)	$E = E_0 e^{V/\Phi}$	E: elastance	19
		E_0: baseline elastance
		V: volume
		Φ: baseline volume
(A14)	$\frac{dq}{dt} = \left(p - p_{out} - Rq + \sigma\frac{dv}{dt} - \sigma_{out}\frac{dv_{out}}{dt}\right)/L$	q: flow through each pulmonary compartment
		p_{out}: pressure of the neighboring compartment
		R: resistance
		σ: viscoelastance
		v: volume
		L: inertance

Valves and Starling resistors

(A15)	$A_e = A_a[M_s\xi(t) + M_r(1 - \xi(t))]$	A_e: effective cross-sectional area	27
		A_a: annulus area	18
		ξ: valve state	20
		M_s, M_r: parameters representing valve condition	
(A16)	$\frac{d\xi}{dt} = K_o(\Delta p(t) - \Delta p_o)(1 - \xi(t))$	If $\Delta p > \Delta p_o$, opening state	
	$\frac{d\xi}{dt} = K_c(\Delta p(t) - \Delta p_c)\xi(t)$	If $\Delta p < \Delta p_c$, closing state	
		K_o, K_c: rate coefficients for opening and closing	
		$\Delta p_o, \Delta p_c$: opening and closing threshold pressures	
(A17)	$\frac{dq(t)}{dt} = \frac{1}{L(t)}(\Delta p(t) - B(t)q(t)|q(t)|)$	q: flow variation across the valve	
(A18)	$\Delta p(t) = p_{up}(t) - p_{down}(t)$	p: pressure difference across the valve length	
(A19)	$L(t) = \frac{\rho l_e}{A_e(t)}$	L: blood inertance	
		ρ: blood density	
		l_e: effective length	

(Continues)

TABLE A1 (Continued)

Model equations		References
(A20) $\quad B(t) = \frac{\rho}{2A_e^2(t)}$	B: Bernoulli's resistance	
Cerebrospinal fluid dynamic		
(A21) $\quad \frac{dp_{IC}}{dt} = \frac{1}{C_{IC}}\frac{dv_{IC}}{dt}$	p_{IC}: intracranial pressure	28
	v_{IC}: total cerebral blood volume	18
(A22) $\quad C_{IC} = \frac{1}{kp_{IC}}$	C_{IC}: intracranial compliance	
	k: elastance coefficient	
Cerebral autoregulation		
(A23) $\quad \tau\frac{dx}{dt} = -x + G\left(\frac{\overline{Q}-\overline{Q}^T}{\overline{Q}^T}\right)$	x: state variable	23
	τ: time constant	29
	G: gain	30
	$\overline{Q}$: time averaged flow	
	$\overline{Q}^T$: reference flow	
(A24) $\quad C = \frac{\overline{C}\{(1-\Delta C/2)+(1+\Delta C/2)\exp[(-x)/k]\}}{1+\exp[(-x)/k]}$	C stands for C_{al}, C_{cp}	
	$\overline{C}$: central value of the sigmoidal autoregulation curve	
	ΔC: amplitude of the sigmoidal autoregulation curve	
	k: constant parameter	
(A25) $\quad \Delta C = 2sat_1, \ k = \overline{C}sat_1$	If $x > 0$ (vasodilation)	
$\qquad \Delta C = 2sat_2, \ k = \overline{C}sat_2$	If $x < 0$ (vasoconstriction)	
	sat_1: constant parameter for upper saturation level	
	sat_2: constant parameter for lower saturation level	
(A26) $\quad \frac{\overline{V}}{\overline{V}^T} = \sqrt{\frac{R^T}{R}}$	$\overline{V}$: mean volume over a cardiac cycle	
	$\overline{V}^T$: mean baseline volume	
	R stands for R_{al}, R_{cp}	
	R^T: baseline resistance	
Baroreflex control		
(A27) $\quad \overline{P}_a = \frac{1}{3}\left(\overline{P}_{rc} + \overline{P}_{lc} + \overline{P}_{aa}\right)$	$\overline{P}_a$: arterial level of activation	31
	$\overline{P}_{r/lc}$: mean right/left carotid artery pressure	24
	$\overline{P}_{aa}$: mean aortic arch pressure	23
(A28) $\quad \overline{P}_v = \overline{P}_{ra}$	$\overline{P}_v$: low-pressure level of activation	25
	$\overline{P}_{ra}$: mean right atrial pressure	
(A29) $\quad n_s = \frac{1}{1+e^{y/k}}$	n_s: sympathetic firing rate	
(A30) $\quad n_p = \frac{1}{1+e^{-y/k}}$	n_p: parasympathetic firing rate	
	$k = -1$: slope of the sigmoidal characteristic at its central point	
(A31) $\quad y = g_a\left(\overline{P}_a - \mu\right) + g_v\left(\overline{P}_v - \delta\right)$	y: linear combination of pressure changes	
	μ: arterial beseline activation level	
	δ: venous baseline activation level	
	g_a, g_v: maximum open loops gains	
(A32) $\quad \frac{dx}{dt} = \frac{1}{\tau}(-x + \sigma)$	x: efferent response (non-dimensional)	
	τ: characteristic time constant	

TABLE A1 (Continued)

Model equations		References
(A33) $\sigma = \alpha n_s - \beta n_p + \gamma$	α, β, γ: parameters from physiological values	
(A34) $\mathcal{P} = \overline{\mathcal{P}} x_{\mathcal{P}}$	Action of x on $\mathcal{P} = \{H, E_{max}, R_a, C_{vn}, V_u\}$	
	With $\overline{\mathcal{P}}$ the setting point value of variable $\mathcal{P}$	

TABLE A2 Table of parameters used in equations presented in Table A1.

Parameters			
1D vessels			20
Blood density	ρ (g/cm^3)	1.06	
Blood dynamic viscosity	μ (P)	0.045	
Reference pressure—arteries	P_0 (mm Hg)	100	
Reference pressure—veins	P_0 (mm Hg)	5	
Tube law parameter—arteries and veins	m (–)	10	
Tube law parameter—arteries and veins	n (–)	−1.5	
Stiffness coefficient	K (dyn/cm^2)	Computed from $\overline{c}_0 = \left(\frac{A_0}{\rho} \frac{\partial p}{\partial A} \Big|_{A=A_0} \right)^{\frac{1}{2}}$	
Reference celerity—arteries	$\overline{c}_0$ (cm/s)	$\overline{c}_0^2 = \frac{2}{3\rho}(k_1 \exp(k_2 r_0) + k_3)$	
Wave speed parameter—arteries	$k_1 \left(\frac{\text{g cm}}{\text{s}^2} \right)$	3×10^6	
Wave speed parameter—arteries	$k_2 \left(\frac{1}{\text{cm}} \right)$	−7	
Wave speed parameter—arteries	$k_3 \left(\frac{\text{gcm}}{\text{s}^2} \right)$	40×10^4	
Reference celerity—veins	$\overline{c}_0$ (cm/s)	$\overline{c}_0 = c_{0,max} - (c_{0,max} - c_{0,min}) \left(\frac{r_0 - r_{min}}{r_{max} - r_{min}} \right)^{\frac{1}{2}}$	
Wave speed parameter—veins	$c_{0,max}$ (cm/s)	400	
Wave speed parameter—veins	$c_{0,min}$ (cm/s)	150	
Wave speed parameter—veins	r_{max} (cm)	0.8	
Wave speed parameter—veins	r_{min} (cm)	0.08	
Wave speed parameter—sinuses	$c_{0,sinus}$ (cm/s)	1500	
Wall viscosity—arteries	γ (dyn/cm^{2}s)	3×10^4	
Wall viscosity—veins	γ (dyn/cm^{2}s)	4×10^3	
Reference wall thickness—arteries	h_0 (cm)	$0.1 \times r_0$	
Reference wall thickness—veins	h_0 (cm)	$0.05 \times r_0$	
Microcirculation			20
Total arterial resistance	$R^T \left(\frac{\text{mm Hg}}{\text{mL}} \right)$	0.85	
Arterial impedance	R_{da}^T (–)	$0.15 R^T$	
Arterioles resistance	R_{al}^T (–)	$0.595 R^T$	
Capillaries resistance	R_{cp}^T (–)	$0.255 R^T$	
Total arterial compliance	$C_{art}^T \left(\frac{\text{mL}}{\text{mm Hg}} \right)$	4	25
Arterioles compliance	C_{al}^T (–)	C_{art}^T	
Capillaries compliance	C_{cp}^T (–)	$0.15 C_{art}^T$	
Total venous compliance	$C_{vn}^T \left(\frac{\text{mL}}{\text{mm Hg}} \right)$	111	25

(Continues)

TABLE A2 (Continued)

Parameters			
Arterial unstressed volume	$V_{u,art}^{T}$ (mL)	615	25
Venous unstressed volume	$V_{u,vn}^{T}$ (mL)	2500	25
Cardiac chambers		RA | RV | LA | LV	20
Active elastance	$E_A \left(\frac{\text{mm Hg}}{\text{mL}}\right)$	0.07 | 0.55 | 0.07 | 2.75	
Passive elastance	$E_B \left(\frac{\text{mm Hg}}{\text{mL}}\right)$	0.04 | 0.05 | 0.09 | 0.12	
Contraction duration	T_{cp} (s)	0.25 | 0.4 | 0.17 | 0.4	
Relaxation duration	T_{rp} (s)	0.17 | 0.15 | 0.17 | 0.15	
Contraction begin	t_c (s)	0.7 | 0.3 | 0.8 | 0	
Relaxation begin	t_r (s)	0.97 | 0.0005 | 0.97 | 0.3	
Viscosity const.	γ (s/mL)	0.0005 | 0.0005 | 0.0005 | 0.001	
Reference pressure	$P_{ch,ini}$ (mm Hg)	5.09 | 5.06 | 6.56 | 8.6	
Unstressed volume	V_u (mL)	20 | 20 | 5 | 5	25
Pericardial parameter	V_{PC} (mL)	400	
Pericardial parameter	Φ_{PC} (mL)	100	
Cardiac valves		Tricuspid | Pulmonary | Mitral | Aortic	20
Valve state parameter	M_s (–)	1 | 1 | 1 | 1	
Valve state parameter	M_r (–)	0.00001 | 0.00001 | 0.00001 | 0.00001	
Opening rate	$K_o \left(\frac{\text{cm}^2\text{s}}{\text{dyn}}\right)$	0.03 | 0.02 | 0.02 | 0.02	
Closing rate	$K_c \left(\frac{\text{cm}^2\text{s}}{\text{dyn}}\right)$	0.04 | 0.02 | 0.04 | 0.02	
Effective length	l_e (cm)	2 | 1.5 | 2 | 1	
Effective area	A_a (cm^2)	6 | 5.7 | 5.1 | 4.9	
Pulmonary circulation		Artery | Capillary | Vein	20
Baseline elastance	$E_0 \left(\frac{\text{mm Hg}}{\text{mL}}\right)$	0.02 | 0.02 | 0.02	
Baseline volume	Φ (mL)	20 | 60 | 200	
Resistance	$R \left(\frac{\text{mm Hg mL}}{\text{s}}\right)$	0.04 | 0.04 | 0.005	
Inertance	$L \left(\frac{\text{mm Hg mL}}{\text{s}^2}\right)$	0.0005 | 0.0005 | 0.0005	
Viscoelastance	$\sigma \left(\frac{\text{mm Hg mL}}{\text{s}}\right)$	0.01 | 0.01 | 0.01	
Unstressed volume	V_u (mL)	60 | 10 | 490	25
Venous valves			20
Valve state parameter	M_s (–)	1	
Valve state parameter	M_r (–)	0.001	
Opening rate	$K_o \left(\frac{1}{\text{mm Hg s}}\right)$	133.32	
Closing rate	$K_c \left(\frac{1}{\text{mm Hg s}}\right)$	40	
Starling resistors			20
State parameter	M_s (–)	0.5	
State parameter	M_r (–)	0.05	
Opening rate	$K_o \left(\frac{1}{\text{mm Hg s}}\right)$	133.32	
Closing rate	$K_c \left(\frac{1}{\text{mm Hg s}}\right)$	133.32	

TABLE A2 (Continued)

Parameters			
Cerebrospinal fluid dynamic			18
Elastance coefficient	$k\left(\frac{1}{mL}\right)$	0.15	
Cerebral autoregulation			32
Time constant	τ (s)	20	
Constant parameter	k (–)	−1	
Gain	G (–)	0.9	
Upper saturation level	sat_1 (–)	0.55	
Lower saturation level	sat_2 (–)	2.0	
Baroreflex control		$H\mid E_{max}\mid R_a\mid C_{vn}\mid V_u$	25
Characteristic time constant	τ (s)	4 | 10 | 15 | 30 | 60	
	α (–)	1.15 | 0.4 | 0.8 | −0.2 | −0.2	
	β (–)	0.34 | 0 | 0 | 0 | 0	
	γ (–)	0.595 | 0.8 | 0.6 | 1.1 | 1.1	
Arterial open loop gain	g_a (mm Hg)	0.02 | 0.02 | 0.02 | 0.02 | 10.8	
Venous open loop gain	g_v (mm Hg)	0 | 0 | 0.7 | 0 | 417	

Note: Values provided for variables controlled by the baroreflex model should be considered as setting point values. The actual value of these variables will change when controlled variables deviate from their setting point. For the definition of parameters that have not been explicitly introduced in this work, please refer to the article indicated in last column.

APPENDIX B

In this appendix, we summarize the main cardiovascular indexes adopted in this work, how they are defined and calculated, in particular those in Tables 2 and 5. All the indexes were evaluated from the numerical solution in the last cardiac cycle of a simulation that had reached a periodic solution. Therefore, in the following list we refer to maximum, minimum and mean values over a cardiac cycle. For one-dimensional vessels computed values are extracted from pressure, flow or velocity waveforms evaluated at the middle-point of the vessel's length.

- SBP: systolic blood pressure; maximum blood pressure.
- DBP: diastolic blood pressure; minimum blood pressure.
- MBP: mean blood pressure; average blood pressure.
- PP: pulse pressure; difference between maximum and minimum blood pressures.
- cfPWV: carotid-femoral pulse wave velocity; it is evaluated with the "foot-to-foot" method as

$$cfPWV = \frac{\Delta L}{\Delta t},$$

where, Δt is the time delay between the arrival of pulse at the right common carotid artery and at the right femoral artery and ΔL is the distance between the two measurement points.

- baPWV: brachial-ankle pulse wave velocity; it is evaluated with the "foot-to-foot" method as

$$baPWV = \frac{\Delta L}{\Delta t},$$

where, Δt is the time interval between the arrival of pulse at the right brachial artery and at the right tibial artery and ΔL is the distance between the two measurement points.

- Augmented P: augmented pressure; it is calculated as the difference between the second and first systolic peaks of aortic pressure.
- Augmentation index; it is calculated as the ratio between augmentation pressure and pulse pressure of aortic root.
- C_a index: total arterial compliance index; arterial compliance index is evaluated as the ratio between stroke volume and brachial pulse pressure, divided by body surface area, taken as 1.92 m^2 for both normotensive and hypertensive subjects.
- HR: heart rate.
- CI: cardiac index; it is calculated as cardiac output divided by body surface area, taken as 1.92 m^2 for both normotensive and hypertensive subjects.
- SI: stroke index; it is evaluated as stroke volume (end-diastolic volume—end-systolic volume of left ventricle) divided by body surface area, taken as 1.92 m^2 for both normotensive and hypertensive subjects.
- E_a: arterial elastance; it is calculated as the ratio between left ventricle end-systolic pressure and stroke volume.
- E_{es}: left ventricle elastance; it is evaluated as left ventricle end-systolic pressure divided by left ventricle end-systolic volume.
- E_a/E_{es}: arterial-ventricular coupling index.
- LV/RV$_{max}$: maximum volume of left/right ventricle.
- LV/RV$_{EF}$: ejection fraction of left/right ventricle; it is calculated as the ratio between stroke volume and end-diastolic volume.
- max/min $\frac{dP}{dt}$: maximum/minimum pressure rate.
- RV-SP: right ventricle systolic pressure.
- RV-EDP: right ventricle end-diastolic pressure.
- M/S/D PAP: mean/systolic/diastolic pulmonary artery pressure, evaluated in the zero-dimensional compartment of the arteries in the pulmonary circulation.
- PI: pulsatility index. It is evaluated from flow waveform or velocity waveform as the difference between the peak systolic and minimum diastolic value, divided by the mean value.
- RI: resistive index. It is calculated from velocity waveform as the difference between peak systolic and peak diastolic velocities divided by peak systolic velocity.